Department of Radio Science and Engineering

Development of Characterization Methods for Antennas and Quasi-Optics

Zhou Du

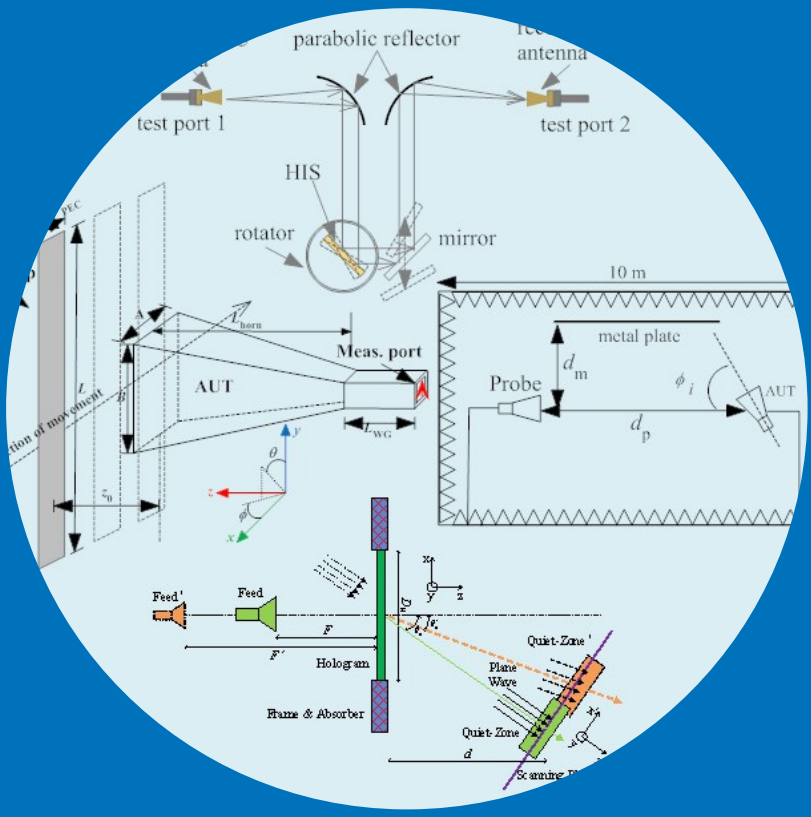

Aalto University

DOCTORAL DISSERTATIONS

Aalto University publication series
DOCTORAL DISSERTATIONS 8/2015

Development of Characterization Methods for Antennas and Quasi-Optics

Zhou Du

A doctoral dissertation completed for the degree of Doctor of Science (Technology) to be defended, with the permission of the Aalto University School of Electrical Engineering, at a public examination held at the lecture hall S1 of the school on 30 January 2015 at 12 noon.

Aalto University
School of Electrical Engineering
Department of Radio Science and Engineering

Supervising professor
Prof. Antti V. Räisänen

Thesis advisors
Dr. Juha Ala-Laurinaho
Asst. Prof. Ville Viikari

Preliminary examiners
Prof. Claire Migliaccio, University of Nice Sophia Antipolis, France
Prof. Manuel Sierra Castañer, Technical University of Madrid, Spain

Opponent
Assoc. Prof. Sergey Pivnenko, Technical University of Denmark, Denmark

Aalto University publication series
DOCTORAL DISSERTATIONS 8/2015

ISBN 978-952-60-6049-1 (printed)
ISBN 978-952-60-6050-7 (pdf)
ISSN-L 1799-4934
ISSN 1799-4934 (printed)
ISSN 1799-4942 (pdf)
http://urn.fi/URN:ISBN:978-952-60-6050-7

Unigrafia Oy
Helsinki 2015

Finland

441 697
Printed matter

Aalto University

Abstract

Aalto University, P.O. Box 11000, FI-00076 Aalto www.aalto.fi

Author
Zhou Du

Name of the doctoral dissertation
Development of Characterization Methods for Antennas and Quasi-Optics

Publisher School of Electrical Engineering

Unit Department of Radio Science and Engineering

Series Aalto University publication series DOCTORAL DISSERTATIONS 8/2015

Field of research Radio Engineering

Manuscript submitted 16 September 2014 **Date of the defence** 30 January 2015

Permission to publish granted (date) 26 November 2014 **Language** English

☐ **Monograph** ☒ **Article dissertation (summary + original articles)**

Abstract

This dissertation focuses on the development of characterization methods for antennas and quasi-optical components.

The dissertation presents three new methods to deal with certain limitations occurred during the antenna measurement processes. First, a new technique using the Chebyshev polynomials has been proposed to process the antenna measurements obtained in non-anechoic sites to obtain equivalent free space radiation patterns. This new technique combines the principle of a FFT-based method with the special relationship between coefficients of the Bessel-Chebyshev polynomials. Experimental results are presented to demonstrate the potential of this approach over conventional time gating techniques for a certain class of problems. Second, a new antenna pattern retrieval method is proposed. In this method, the antenna reflection coefficient is measured many times when a unique reflective load with known spatial reflection properties is placed near the antenna in each measurement. The antenna pattern is obtained from the measurements with an inversion algorithm. Simulations have been used to verify the theoretical basis and the method has been experimentally demonstrated at 30 GHz. The results show that the method could enable sufficient accuracy with low gain antennas or in the vicinity of main lobe with directive antennas. Third, a new technique is presented to realize a wideband hologram compact antenna test range (CATR) by linearly adjusting the feed location. The wideband formulas for linearly adjusting the feed have been discussed and verified. The performance of the wideband operation has been demonstrated by the measured results at W (95 GHz) and D (170 GHz) bands for the hologram aperture diameter of 350 mm.

The dissertation also discusses characterization of quasi-optics, namely, MEMS-based high-impedance surface (HIS) and reflectarray elements. First, the reflection properties of the single unit cell structure of MEMS-based HIS is studied, tunability of the MEMS varactors and beam steering of a large structure at 80 GHz has been demonstrated with a simplified model. The structure allows steering of the beam within the range from -45° to +45°. A quasi-optical measurement setup has been built for the experimental characterization. Second, the design and optimization process of reconfigurable reflectarray element integrated with MEMS-based phase shifter at 120 GHz is studied. Also, the dielectric properties of SU-8 substrate have been characterized with on-wafer measurements. Several design parameters which could affect the modulation efficiency have been studied.

Keywords antenna measurement, pattern retrieval, reflection coefficient, compact range, high-impedance surface, MEMS, reflectarray element

ISBN (printed) 978-952-60-6049-1 **ISBN (pdf)** 978-952-60-6050-7

ISSN-L 1799-4934 **ISSN (printed)** 1799-4934 **ISSN (pdf)** 1799-4942

Location of publisher Helsinki **Location of printing** Helsinki **Year** 2015

Pages 124 **urn** http://urn.fi/URN:ISBN:978-952-60-6050-7

Preface

The research in this dissertation has been mainly carried out at the Dept. of Radio Science and Engineering of Aalto University (former Helsinki University of Technology).

First, I would like to express my sincere gratitude to my supervisor, Prof. Antti Räisänen for accepting me as a doctoral student in his group and for his trust, encouragement, support, immense knowledge, and guidance during these years. My two instructors/thesis advisors deserve special thanks. Dr. Juha Ala-Laurinaho, thank you for your instructions, fruitful discussions, practical skills which you shared to me, and especially for your rigorous working attitude which I learned during these years. Prof. Ville Viikari, many thanks to you for your patience, inspiration, and for always being open to discuss new ideas and guiding me to find solutions in the project throughout the final phase of my doctoral studies. It is my great honor and pleasure working with you and this will definitely be my most cherish moment in Aalto University.

I warmly thank my main collaborators, Dr. Dmitry Chicherin, Dr. Aleksi Tamminen, and Dr. Zhiping Li (from Beihang University, Beijing, China) for our nice collaborations during the research. My thanks go to my present and former colleagues at the Dept. of Radio Science and Engineering for their help and discussions, Afroza, Aki, Azremi, Clemens, Jinsong, Juha M, Katsu, Krista, Linsheng, Reza, Sathya, Subash, Tommi, and many more. The help from support personnel is appreciated for providing an enjoyable place to work in. Thank you Eikka, Lauri, Lorenz, Mirjam, Sari, Stina, Timo, Tuula, Viktor.

I would like to thank the pre-examiners of my dissertation, Prof. Manuel Sierra Castañer and Prof. Claire Migliaccio for their valuable reviews and insightful comments to improve the quality of this dissertation. My appreciation also goes to Prof. Sergey Pivnenko for accepting to be the opponent during the public examination.

Prof. Jinhwan Koh from Gyeongsang National University, Jinju, South Korea deserves thanks for his continuous support after I moved to Finland.

Finally, my deepest thanks go to my family. Without their support and love, I could not be on this stage. To my parents, thank you for your unconditional support and encouragement during these years. To my dear wife HeLi (pang pang), thank you for your endless love, support, encouragement, and understanding, especially when I was in a difficult time. You will always be my strong backing and I will be yours. To our little girl Eden, thank you for joining our family at this very special moment! You brought us a lot of happiness and we love you so much!

Espoo, Dec. 22, 2014

Zhou Du

谨以此博士论文献给：

亲爱的父母，父爱如山，母爱如水，感谢你们赐予我生命，生活中给与我无尽的关爱和支持，老爸，老妈，我爱你们！！

挚爱的妻子，最美好的年华，遇到最美好的你，感谢有你一路陪伴，给我一个温暖的家！致我们共同经历的求学生涯！胖胖，我爱你！！

杜舟

二零一四年十二月二十二日

芬兰，埃斯波

Contents

List of Abbreviations

1D	1 dimensional / 1 dimension
2D	2 dimensional / 2 dimensions
3D	3 dimensional / 3 dimensions
AUT	Antenna under test
BW	Bandwidth
CATR	Compact antenna test range
CB-CPA	Conductor-backed coplanar patch antenna
CB-CPW	Conductor-backed coplanar waveguide
CGM	Conjugate gradient method
CPA	Coplanar patch antenna
CPW	Coplanar waveguide
DC	Direct current
EU	European Union
FFT	Fast Fourier Transform
FP7	The Seventh Framework Programme
HCATR	Hologram-based compact antenna test range
HFSS	High frequency structural simulator
HIS	High-impedance surface
KTH	Kungliga Tekniska Högskolan / Royal Institute of Technology
MEMS	Microelectromechanical systems
MMID	Millimeter-wave identification
PEC	Perfect electric conductor
PP	Peak-to-peak (derivation of the amplitude and phase response in quiet-zone)

RCS	Radar cross section
RF	Radio frequency
RFID	Radio-frequency identification
SEM	Scanning electron microscopy
TD	Time delay
TEKES	Innovaatiorahoituskeskus / Finnish Funding Agency for Innovation
VTT	Teknologian tutkimuskeskus VTT / VTT Technical Research Centre of Finland
WR	Waveguide rectangular

List of Symbols

a_n	Expansion coefficient of the polynomials
A	Aperture dimension of the pyramidal horn antenna
$A_{initial}$	Initial guess of the amplitude
B	Aperture dimension of the pyramidal horn antenna
c	Speed of light
d	Distance between hologram and the quiet-zone
d_{m}	Parallel separation between the metal plate and the AUT/probe
d_{p}	Distance between the probe and the AUT
D	Largest dimension of the AUT aperture
D_H	Dimension of the hologram
D_{move}	Relative moving distance of reflective load
E	Electric field
E_{o}	Specular reflection of the electric field of the reflectarray element
$E_{\mathrm{AUT}}(x, y, z)$	Electrical aperture distribution at the plane z
E_{m}	Modulated electric field of the reflectarray element
$E_{\Gamma}(x, y, z)$	Field reflected from the reflective surface at the plane z
f_o	Resonance frequency
f_{M2}	Frequency index
F	Focal length
F'	Adjusted focal length
G	Gap between patch and ground
G_{f}	Gap between signal strip and ground
H	Horizontal polarization
l_2	Frequency scaling factor

L	Length of the reflective load
L_f	Length of CPW feed line
L_{horn}	Flare length of the pyramidal horn antenna
L_p	Reflectarray element patch length
L_{WG}	Waveguide length of the pyramidal horn antenna
M	Scaled value in wideband HCATR
M_2	The number of the frequency domain data
N	Number of degree in the polynomials
R	Reflection coefficient
S	Aperture surface
S_{11}	Reflection coefficient referenced to the antenna feed
$S_{11,\ aperture}$	Reflection coefficient referenced to aperture plane of a lossless and perfectly matched antenna
$S_{11,\ static}$	Constant term in reflection coefficient due to impedance mismatch
$S_{21}(f,\phi)$	Transmission coefficient / Frequency and angular domain response
$S_{21}(t,\phi)$	Transmission coefficient / Temporal and angular domain response
S-parameter	Scattering parameter
T_n	Chebyshev polynomials of the first kind
U_{n-1}	Chebyshev polynomials of the second kind
V	Vertical polarization
W	Reflectarray element spacing
W_f	Reflectarray element signal strip width
W_p	Reflectarray element patch width
W_{PEC}	Width of the reflective load
x	Cartesian coordinate
$X(f_{M2})$	Frequency response at f_{M2} (for different azimuth angles ϕ_i)
y	Cartesian coordinate
z	Cartesian coordinate
z_o	Offset distance
Z_g	Capacitive grid impedance due to the adjacent metal patches

Z_{pp}	Capacitive impedance due to the parallel-plate capacitor
Z_s	Inductive impedance
Z_{tot}	Total input impedance
α	Attenuation constant between antenna feed and aperture plane
$\Gamma(x, y)$	Spatial reflection coefficient
Δf	Bandwidth
η_m	Modulation efficiency of the reflectarray element
θ_c	Direction of plane wave propagation after collimation
θ_d	Phase delay between antenna feed and aperture plane
$\theta_{initial}$	Initial guess of the phase
θ_{valid}	Valid angular region
λ	Wavelength
λ_g	Guided wavelength used in reflectarray element design
ϕ_i	Azimuth angle

List of Publications

This doctoral dissertation consists of a summary and of the following publications which are referred to in the text by their Roman numerals.

I. Z. Du, D. Chicherin, and A. V. Räisänen, "Millimeter wave beam steering with a MEMS-based high impedance surface," in *Proc. 41st European Microwave Conference,* Manchester, UK, Oct. 10-14, 2011, pp. 1043-1046.

II. Z. Du, J. Ala-Laurinaho, D. Chicherin, A. V. Räisänen, M. Sterner, and J. Oberhammer, "Reflection phase characterization of the MEMS-based high impedance surface," in *Proc. 42nd European Microwave Conference,* Amsterdam, The Netherlands, Oct. 29 – Nov. 1, 2012, pp. 617-620.

III. Z. Du, A. Tamminen, J. Ala-Laurinaho, J. Säily, P. Rantakari, A. Luukanen, and A. V. Räisänen, "Design and optimization of reconfigurable reflectarray element with MEMS phase shifter," in *Proc. 7th European Conference on Antenna and Propagation*, Gothenburg, Sweden, Apr. 8-12, 2013, pp. 2422-2426.

IV. Z. Du**,** J. Moon, S. Oh, J. Koh, and T. K. Sarkar, "Generation of free space radiation patterns from non-anechoic measurements using Chebyshev polynomials," *IEEE Transactions on Antennas and Propagation,* vol. 58, no. 8, pp. 2785-2790, Aug. 2010.

V. Z. Du, V. Viikari, J. Ala-Laurinaho, A. Tamminen, and A. V. Räisänen, "Antenna pattern retrieval from reflection coefficient measurements with reflective loads," *Progress in Electromagnetics Research*, vol. 148, pp. 15-22, 2014.

VI. Z. Du, V. Viikari, J. Ala-Laurinaho, and A. V. Räisänen, "2D antenna radiation pattern retrieval using reflection coefficient measurements," in *Proc. 2014 Asia-Pacific Microwave Conference (APMC2014)*, Sendai, Japan, Nov. 4-7, 2014, pp. 846-848.

VII. Z. Li, J. Ala-Laurinaho, Z. Du**,** and A. V. Räisänen, "Realization of wideband hologram compact antenna test range by linearly adjusting the feed location," *IEEE Transactions on Antennas and Propagation*, vol. 62, no.11, pp. 5628-5633, Nov. 2014.

Author's Contribution

Publication I: "Millimeter wave beam steering with a MEMS-based high impedance surface"

The work was mainly done by the author. The author had the main responsibility for developing the idea and was responsible for writing the manuscript. Dr. Dmitry Chicherin participated in analysing the results, measured the *S*-parameters and instructed the work.

Publication II: "Reflection phase characterization of the MEMS-based high impedance surface"

The work was mainly done by the author. The author had the main responsibility for developing the idea and was responsible for writing the manuscript. Dr. Juha Ala-Laurinaho participated in analysing the results and instructed the work.

Publication III: "Design and optimization of reconfigurable reflectarray element with MEMS phase shifter"

The work was mainly done by the author. The author had the main responsibility for developing the idea and was responsible for writing the manuscript. Dr. Aleksi Tamminen measured the SU-8 photoresist characteristics. Dr. Juha Ala-Laurinaho participated in analysing the results and instructed the work.

Publication IV: "Generation of free space radiation patterns from non-anechoic measurements using Chebyshev polynomials"

The work was mainly done by the author. The author had the main responsibility for developing the idea and was responsible for writing the manuscript. The author formulated the methods in detail and carried out data post-processing and analysis. Dr. Jung Ick Moon and Dr. Soon-soo Oh provided the antenna measurement results. Prof. Jinhwan Koh participated in analysing the results, instructed and supervised the work.

Publication V: "Antenna pattern retrieval from reflection coefficient measurements with reflective loads"

The work was mainly done by the author. The author had the main responsibility for developing the idea. The author formulated the methods in detail, carried out simulations, measurements, data post-processing and analysis. Prof. Ville Viikari and Dr. Juha Ala-Laurinaho participated in analysing the results and instructed the work.

Publication VI: "2D antenna radiation pattern retrieval using reflection coefficient measurements"

The work was mainly done by the author. The author had the main responsibility for developing the idea and was responsible for writing the manuscript. The author carried out simulations, data post-processing and analysis. Prof. Ville Viikari participated in analysing the results and instructed the work. Dr. Juha Ala-Laurinaho instructed the work.

Publication VII: "Realization of wideband hologram compact antenna test range by linearly adjusting the feed location"

This is a result of collaborative work. Dr. Zhiping Li had the main responsibility for developing the research idea. The author was involved in simulations, measurements and analysis of the results. Dr. Juha Ala-Laurinaho participated in analysing the results and instructed the work.

1. Introduction

1.1 Background, Motivation and Objectives

The antenna is an electrical device (usually a metallic structure) with the function of transforming guided electromagnetic signals into electromagnetic waves propagating in free space. Typically, the antenna can be used as either a receiving or transmitting component. The antenna may also include additional reflective elements or surfaces to direct the radio waves into a beam or other desired radiation pattern [1].

Millimeter and sub-millimeter wave antennas have recently become available even for relatively low-cost applications due to advances in lithographic techniques. Recent development of RF MEMS (microelectromechanical systems) has also enabled tunable and reconfigurable mm/submm-wave antennas [2]. Use of such antennas are proposed for various applications, e. g. automotive radar in 79 GHz band (77-81 GHz) in European Union (EU) for the advantage of compact size, decreased weight and small emission power needed [3], and the electrically controlled reconfigurable reflectarray for millimeter-wave identification and radar application [4], [5], etc. Several collaborative projects have been devoted to the research of the aforementioned purposes also in Finland. An EU Seventh Framework Programme (FP7) project TUMESA (MEMS tunable metamaterials for smart wireless applications) was carried out during 2008-2011. The main objective was to develop novel on-chip phase shifting and beam steering devices based on MEMS tunable high-impedance surfaces (HIS) [7], [8]. A NORDITE ICT project for automotive radar at 77 GHz in 2006-2010 focused on the utilization of RF MEMS technology for automotive radar sensors. A project funded by Tekes focusing on silicon based millimeter wave identification (MMID) system for imaging, sensing, and wireless communication applications (SIMIDS) was carried out during 2010-2013 between Aalto University and VTT (Technical Research Centre of Finland).

Some quasi-optical components, e.g. MEMS-based HIS structure and reflectarray elements are crucial in these projects. Therefore, numerical and experimental characterizations of these components are a necessary and unavoidable step. In addition to the contribution in this dissertation [I]-[III], some researches are reported in [4]-[12],

Traditionally the antenna is measured in far-field or near-field, or in a compact antenna test range (CATR). In principle, any antenna could be successfully measured using the aforementioned methods with proper implementation. However, the options of choosing one method over the other depend on the surrounding environment, cost of facilities, electrical dimensions of the antenna, etc. Furthermore, each measurement technique has certain advantages and limitations. The main research interests of this dissertation are to solve to following issues [IV]-[VII], [13], [14]:

- In the far-field technique, a reference antenna is placed in the far-field of the antenna under test (AUT). The transmission between the AUT and the reference antenna is then recorded at different rotations of the AUT. The measurement is typically performed in an anechoic chamber to avoid reflections. The purpose of employing an anechoic chamber is to eliminate the reflected field components emanating from the measurement enclosures so that the measured radiation pattern corresponds to the case when similar data can be generated for the antenna in free space conditions. Several mature signal processing methodologies have been applied to further improve the quality of the data measured in moderately good anechoic conditions [15]-[17]. However due to practical and monetary constraints it is not always possible to emulate a perfect anechoic environment. The objective is to further study the methods that may eliminate the undesired reflections measured in non-anechoic conditions through processing of the measured data [IV].
- In the CATR technique, a nearly planar wavefront representing far-field conditions is generated with a collimating element in a very short distance compared to the generally known far-field limit of $2D^2/\lambda$. The collimating element can be a reflector or a lens. At higher frequencies, manufacturing of a hologram is easier than that of a reflector or lens surfaces because of the two-dimensional planar structure and the surface accuracy requirement. Consequently, a hologram CATR is very attractive for antenna measurement at mm/submm-wave bands [18]-[26]. However, as a frequency sensitive element, the operating bandwidth is usually limited

to ± 5%-10% [26]. One objective of the dissertation is to develop a technique to realize a wide band hologram-based CATR [VII].

- In any of the aforementioned methods, antennas are connected to the measurement equipment with cables that, when moved or rotated, easily change their properties, such as the electrical length. At high frequencies, even a small relative change in the geometry or dimensions of the cable may cause a huge phase change to the transmitted signal, as the cable can be electrically very long. The objective is then to develop a method for antenna measurement avoiding flexing cables and antenna movements [V], [VI].

1.2 Contents of the Dissertation

A transmitting or receiving radio system includes always an antenna, but this antenna may be either a clearly separate, independent device or an integrated item with other radio electronics, or something between. Furthermore, an antenna may be an element antenna, an array of element antennas, or in case of reflector and lens antennas, a combination of an illuminating antenna and the main focusing element.

In order to provide a desired illumination of the main focusing element, a quasi-optical system is needed. The versatility of the antenna concept as described above means that in order to be able to understand and design various antenna systems, a very versatile set of different characterization methods is needed. This dissertation discusses several of these methods, ranging from characterization of an element antenna and quasi-optical component to the measurement methods of large antenna systems.

The contents of this dissertation are organized as follows: Chapter 2 and Chapter 3 are devoted to numerical investigation of MEMS-based HIS and reflectarray elements. Particularly, Chapter 2 is focused on the feasibility study of the beam steering and reflection phase properties of the MEMS-based tunable HIS. The stability of the optimized structure for the desired frequency is examined. Numerical and experimental analyses of the large impedance surface for different angle of incidence are presented. Chapter 3 is focused on the design and optimization of reflectarray elements using SU-8 as its dielectric substrate material.

Chapter 4 is devoted to deal with certain limitations occurred during different antenna measurement processes (as mentioned in Section 1.1). Several new methods have been presented and discussed.

The summary of the publications describing the contributions of this dissertation is presented in Chapter 5. Chapter 6 presents conclusions and future work.

1.3 Scientific Contributions

The scientific merits of this dissertation are:

1. The beam steering capacity of a large MEMS-based HIS has been numerically demonstrated with a simplified model at W band. The reflection properties of the MEMS-based HIS have been characterized numerically and a quasi-optical measurement setup has been built for the experimental characterization [I], [II].

2. The design and optimization process of the reconfigurable reflectarray element with MEMS-based phase shifter at 120 GHz is studied [III].

3. A new technique using the Chebyshev polynomials has been proposed to process the antenna measurements obtained in non-anechoic sites to obtain equivalent free space radiation patterns [IV].

4. A new antenna pattern retrieval method from reflection coefficient measurements with reflective loads has been proposed [V], [VI].

5. A new technique has been presented to realize the wideband hologram compact antenna test range by linearly adjusting the feed location [VII].

2. Characterization of MEMS-Based High-Impedance Surface

The mushroom-type HIS was first introduced by Sievenpiper in 1999 [27]. It is a type of metallic electromagnetic structure with high effective surface impedance. Such surface is capable to suppress the propagating surface waves within a particular frequency range and reflect the incident plane waves with no phase reversal. Conventionally, it is formed by a sheet of electrically small metal patches with or without vertical conducting vias connecting to metal ground plane and the size of each patch is much smaller than the wavelength of interest.

The HIS structure and its variations have attracted a lot of interest since it was proposed, and they have been used in many applications. As an example, the HIS was used to serve as the finite ground plane instead of a traditional metal sheet to improve the antenna radiation pattern [28]. Another example is in portable handset communications where it serves as a shield between the antenna and the user to improve the antenna radiation efficiency and extend the battery life [29].

This section is organized as follows. Section 2.1 introduces the beam steering applications of HIS and Section 2.2 presents the MEMS-based HIS for mm/submm-wave frequencies. The beam steering is demonstrated by simulation in Section 2.3. Section 2.4 presents the numerical and experimental studies of the reflection phase of the MEMS-based HIS.

2.1 Beam Steering using High-Impedance Surface

The mechanical beam steering application of HIS was introduced in [30], in which the reflected plane wave on the HIS was steered by adding a layer of adjustable plates overlapping the stationary ones and mechanically moving or tuning the layer position with respect to the surface to generate the needed reflection phase gradient. The electronic beam steering of HIS was elaborated in [31] and experimentally verified in [32] and then extended for two-

dimensional (2D) beam steering for both polarizations [33] by introducing the reverse-biased varactor diodes connected between each adjacent pairs of the array on the surface. The effective capacitance between two neighbouring cells, and consequently the effective input impedance and resonance frequency could be changed by applying the bias voltage to the varactor diodes. Therefore, a gradient of the reflection phase was created by adjusting the bias voltage through the whole surface and the reflected beam was electronically steered with different combination of the bias voltages. The steered angular range at 4.5 GHz from -40° to +40° at both polarizations was achieved with an average gain of 14 dBi and an average beamwidth of 15°.

2.2 MEMS-based High-Impedance Surface

As mentioned in Section 1.1, an EU FP7 project TUMESA was devoted to develop novel on-chip phase shifting and beam steering devices based on MEMS tunable HIS for automotive radar application in 79 GHz band. This section presents the relevant findings of the project.

MEMS fabrication techniques have been developed since the 1970s for pressure and temperature sensors, etc. [2]. At millimeter and sub-millimeter wave frequencies, the MEMS elements have been demonstrated as a relatively mature technique due to its relatively small feature size and low losses compared to other conventional solutions. Artificial electromagnetic materials normally consist of a set of structural elements in an orderly arrangement [34], i.e. arrays, and they usually exhibit advantageous electromagnetic properties. From this point of view, a lattice of HIS is a particular case of artificial electromagnetic materials.

Combining these features provided by the MEMS and the concept of artificial HIS structures, a novel MEMS-based tunable HIS was proposed in 2006 [35]. It was applied to a phase shifter at millimeter and sub-millimeter wavelengths, in which the proposed HIS was placed along the narrow walls of a rectangular metal waveguide to affect the propagation constant, and then consequently changed the phase of the propagating wave. Later the MEMS-based HIS was introduced in a rectangular metal waveguide to create a reflection type phase shifter [36], [37] and in a dielectric rod waveguide [38]. Figure 2.1 shows a schematic layout of a unit cell of the MEMS-based HIS for beam steering application [I]. The nominal design parameters are listed in Table 2. 1.

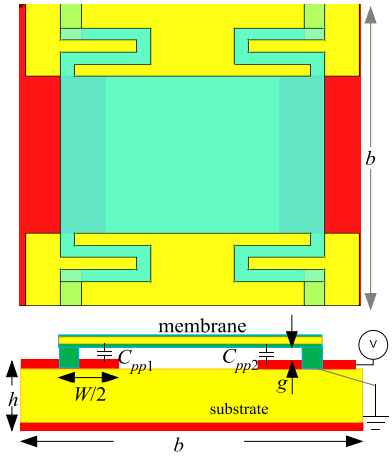

Figure 2.1 Top and side view of unit cell of the MEMS-based HIS [I].

Table 2. 1 Nominal design parameters shown in Figure 2.1 for beam steering applications.

Parameters	*b*	*g*	*h*	*W*
Value	350 µm	1.8 µm	110 µm	130 µm

2.3 Beam Steering with MEMS-Based High-Impedance Surface

The MEMS-based HIS is a multi-layer structure. It consists of an array of electrically small MEMS parallel-plate capacitors, in which the top plate is suspended by springs. The basic idea of the proposed variable capacitor is that application of a bias voltage between the membrane and the bottom plate of the MEMS varactor changes the distance between them, which in turn changes the effective capacitance of the whole structure affecting the resonance frequency of the HIS. It is also possible to introduce an actuation electrode whose thickness is smaller than that of the bottom plate (see Figure 2.2(a)). MEMS-based tunable HIS is a periodic array of unit cells with at least 5 x 5 cells (see Figure 2.2(b) for 3x3 array).

2.3.1 Equivalent Circuit and Surface Tunability

The effective input impedance of the MEMS-based HIS can be interpreted as the parallel connection of the following three impedances [39]:

- The capacitive grid impedance Z_g due to the adjacent metal patches,

- The capacitive impedance Z_{pp} due to the parallel-plate capacitor between the upper membrane and the lower patches,
- The inductive impedance Z_s due to the thin grounded dielectric layer.

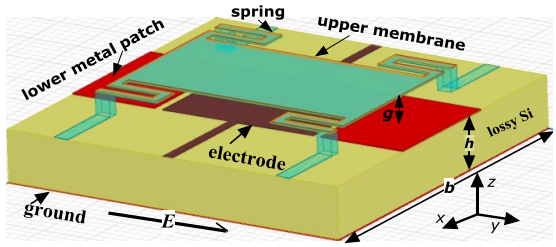

(a)

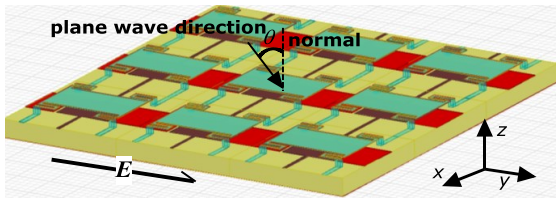

(b)

Figure 2.2 MEMS-based HIS: (a) unit cell (with actuation electrode); (b) example of a 3x3 array (not to scale) [II].

For detailed interpretation of each impedance, see [I], [II]. Figure 2.3 shows the equivalent transmission line model which indicates that the total input impedance Z_{tot} equals to

$$Z_{tot} = (Z_s^{-1} + Z_{pp}^{-1} + Z_g^{-1})^{-1}. \quad (2.1)$$

This equivalent circuit can be used to calculate the reflection coefficient R of the incident electric field at the reflecting surface in terms of Z_{tot} *and* Z_0.

$$R = (Z_{tot} - Z_0) / (Z_{tot} + Z_0). \quad (2.2)$$

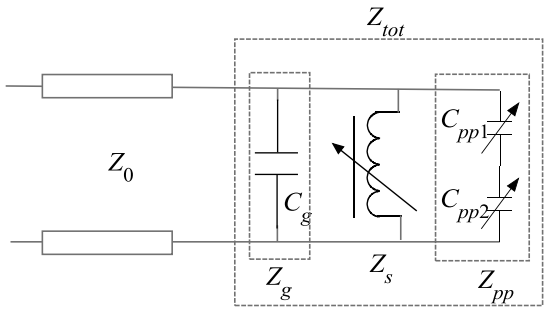

Figure 2.3 Equivalent circuit model of the single unit cell structure [I], [II].

The beam steering can be achieved by programming the gradient of the reflection phase as a function of the gap between the membrane and the lower patches, which influences the effective surface input impedance.

HIS array is a periodic structure and its electromagnetic performance can be simulated with simplified single unit cell with appropriate boundary conditions. The tunability has been numerically studied with Ansoft HFSS™ full wave 3D simulation software, in which two electric boundaries are assigned on two opposing walls on *x-y* plane and two magnetic boundaries on *y-z* plane [I].

Figure 2.4 shows simulation results of the reflection phase of the MEMS tunable HIS for different values of the gap of the MEMS varactor. It indicates that, by varying the gap to certain values, the resonant frequency is tuned approximately from 70 GHz to 100 GHz. The maximum tuning range achieved at 80 GHz is shown in right-hand side of Figure 2.4.

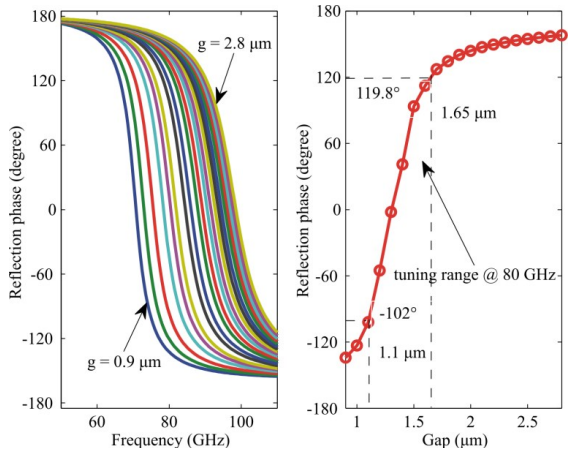

Figure 2.4 Reflection phase for single unit cell with 75 µm substrate thickness as a function of frequency and gap (structure with electrode), simulated [I].

2.3.2 Reflective Strip Beam Steering

The MEMS tunable HIS can be used for electronic reflective beam steering by inducing reconfigurable surface impedance through application of different bias voltage to different rows of elements of the MEMS varactor array. Since full-wave simulation of electrically large reflective surface with electrically small features of MEMS varactors is computationally an extremely large problem, a simplified model of a surface with strips formed by 40 impedance elements of dimensions 0.35 x 0.35 mm² is used (see Figure 2.5). Configuring the surface so that different strips have different impedances and different

phase of the reflection coefficient, the reflected beam can be steered by changing the gradient of the surface impedance.

Theoretically, the reflection phase of the neighbouring strips can be chosen arbitrary taking into account 360° invariance. In the case of MEMS tunable HIS, the tuning range of the MEMS tunable HIS is restricted by the limited surface tunability which in turn limits the beam steering capability of the whole HIS array. Figure 2.6 shows an example of the required reflection phase impedances with incident angle from 45° and reflective beam to be steered to 0°. In order to model a planar array condition, 20 similar linear arrays with 0° phase shift are added in the *z*-direction. When a wave impinges to a flat surface obliquely, it will generate backward and forward reflected wave (see Figure 2.5) and these waves contribute to the side lobe level at particular angles.

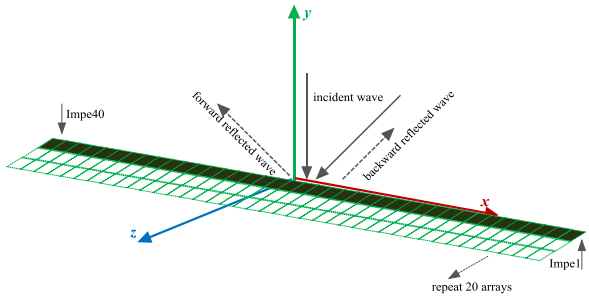

Figure 2.5 40 impedance elements in the open boundary conditions, normal and 45° off broadside incidence are excited to the surface [I].

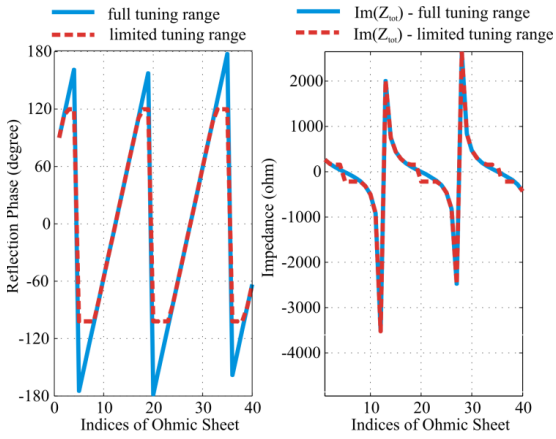

Figure 2.6 The required reflection phase impedances with incident angle from 45° and reflective beam to be steered to 0° [I].

Figure 2.7 shows a normalized radiation pattern of the steered beam desired for -30°. The steered angle of the main lobe agrees well with the programmed value, meanwhile, the side lobes still need to be optimized, i.e. the forward and backward reflections. The results for other incidence and steering angles are obtained in [I].

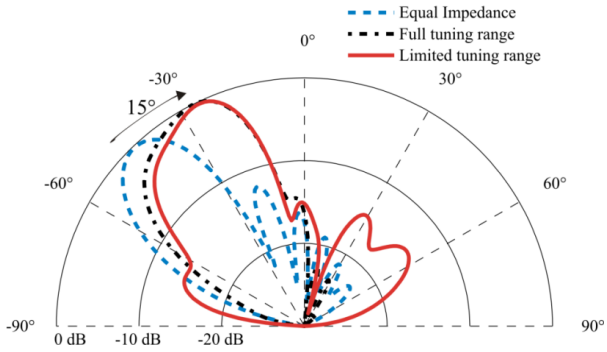

Figure 2.7 The normalized radiation pattern at 80 GHz with incident angle of 45° for the surface which is programmed for -30° [I].

2.4 Reflection Phase Characterization of MEMS-Based HIS

The reflection phase feature attracts the most interest of the special properties of the multilayer HIS structure. The reflection phase is defined as the phase of the reflected electric field monitored at the surface. In this section, we present the numerical analysis of the reflection properties of a MEMS-based HIS array (with actuation electrode and a frozen membrane) when changing the angle of incidence of the beam, and examine the stability of the optimized structure for the desired operational frequency band. In addition, a quasi-optical measurement setup is presented for measuring the reflection coefficient from different oblique angles of incidence with a network vector analyser.

In order to characterize the reflection coefficient of the HIS illuminated by an obliquely incident plane wave, the full wave simulator (Ansoft HFSS™) is used to construct the geometry of the unit cell and collect the reflection data. Periodic boundary conditions are applied to the unit cell structure in x- and y-directions to mimic an infinite array situation (see Figure 2.2(a)), and observation plane is positioned at $0.55\lambda_{80\text{GHz}}$ above the ground. The periodic structure studied in this section is realized with silicon substrate with loss tangent of 0.015. The unit cell of the multi-layer HIS consists of two lower metal patches separated in E-field direction and of a metal upper membrane suspended by 2 μm above the patches with a spring structure. The width of the membrane along the E direction is 225 μm, the half-length of the lower patch

is 78 μm, and the height of the silicon substrate is 110 μm; the parameters are optimized for operation at 84 GHz.

The simulated reflection properties of the unit cell of the MEMS-based HIS for different angles of incidence are shown in Figure 2.8. The reflection phase of the unit cell surface varies continuously from about 140° to -150° versus frequency. Figure 2.9 shows the resonance frequency and the relative bandwidth versus the angle of incidence of the unit cell. Both are slightly increasing with the increase of θ, and most of the resonance frequencies lie within the desired 84 GHz band. This means that the angle of incidence has weak effects to the resonance frequency of the surface impedance. The bandwidth of the resonance is defined as the range where the reflection phase falls between 90° and -90°, meanwhile the relative bandwidth is the ratio between the bandwidth and the resonance frequency $\Delta f / f_0$.

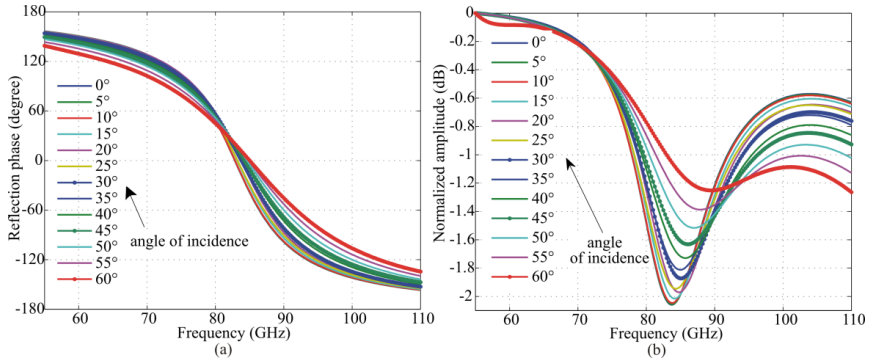

Figure 2.8 Simulated reflection properties of the unit cell of MEMS-based HIS for different angles of incidence: (a) phase; (b) amplitude [II].

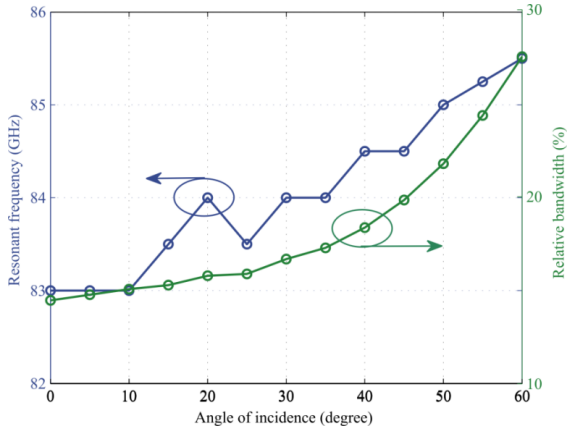

Figure 2.9 Resonance frequency and the relative bandwidth versus angle of incidence [II].

2.4.1 Quasi-Optical Measurement Setup

The manufactured HIS prototype is an array of 200 x 52 unit cells with a periodic length of 350 μm as shown in Figure 2.10. The HIS prototype has been manufactured by Royal Institute of Technology (KTH) Sweden. The extra electrode is introduced underneath the top membrane (see Figure 2.2 and Figure 2.10) and the resonance frequency is estimated to be at 84 GHz [7]. The structure is frozen, i.e. the MEMS membranes are not actuated during the measurements.

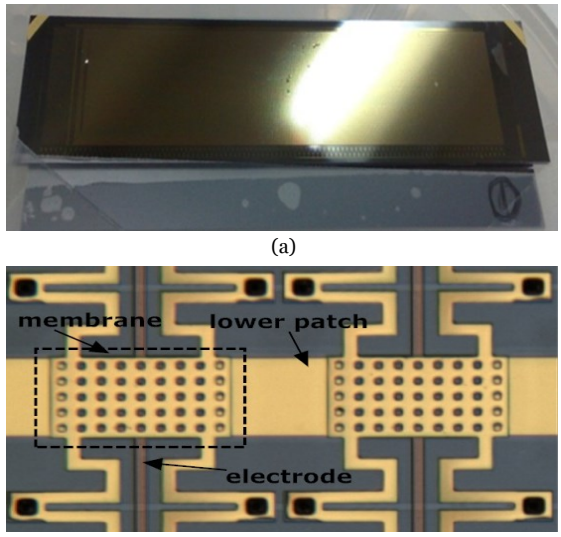

(a)

(b)

Figure 2.10 Manufactured MEMS-based HIS: (a) optical image; (b) scanning electron microscopy (SEM) image [II].

A quasi-optical measurement setup has been built for measuring the reflection phase of the MEMS-based HIS array with three different angles of incidence. Figure 2.11 shows the schematic design of the setup and Figure 2.12 shows the photograph of the measurement setup. Two standard horn antennas with a very narrow beam are mounted at test ports 1 and 2 and thus acting as the transmitting and receiving antennas. In addition, two parabolic reflectors are used to collimate and focus the transmitted waves. The HIS acts as a reflector and it is fixed on the rotator. The angle of incidence is defined by tuning the rotator. Meanwhile, a flat mirror is mounted on a carrier rail in order to position it properly with respect to the corresponding angle of incidence. With the proposed setup, for a chosen angle of incidence and a fixed polarization, the transmission coefficient of the HIS under test and the reference aluminium plate is recorded through two test ports by the HP8510

vector network analyzer. Due to the facility restriction, only three oblique angles of incidence are chosen, they are 30°, 45°, and 60°.

In order to calibrate the retrieved reflection phase properties, the Fourier transform analysis is needed to calculate the transmission path length. The nominal thickness of the HIS embedded in a holding pad is 1.47 mm and the thickness of the aluminum plate is 1 mm. The phase of the wave travelling in the above-mentioned path lengths should be calibrated out in order to restore the true reflection phase of the surface.

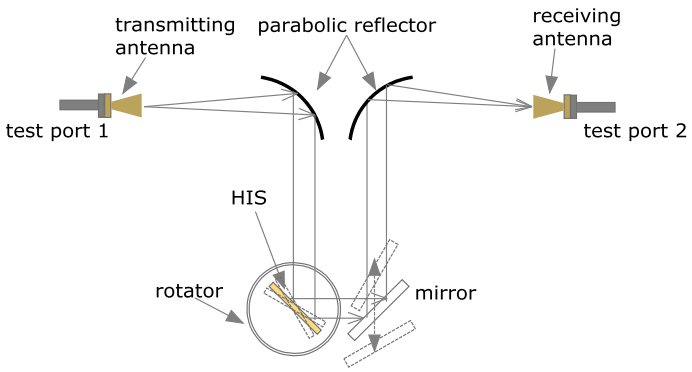

Figure 2.11 Schematic design of the quasi-optical measurement setup [II].

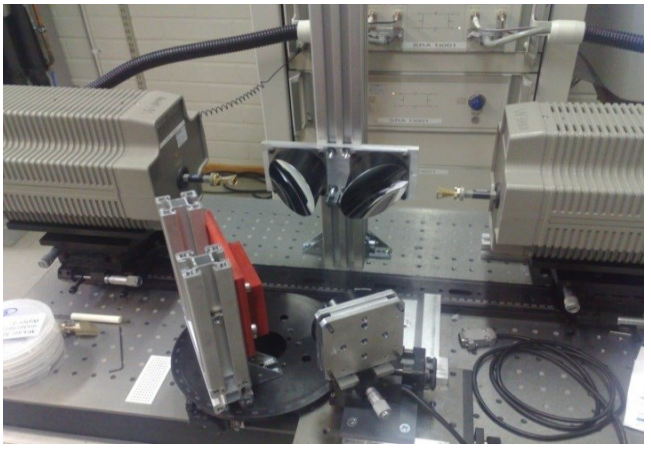

Figure 2.12 Photograph of the quasi-optical measurement setup, see [II] for the details of the HIS holder and chip.

The normalized measured reflection amplitude of the MEMS-based HIS array is shown in Figure 2.13(a). The normalization is carried out by subtracting the amplitude of the measured reflection amplitude of the reference aluminum plate. Because of the restriction of the frequency range in the measurements (75-110 GHz in WR-10 band), it is not comparable to the

whole frequency band of the simulation result. The 9th degree polynomial fitting is used to smooth the rapid variation of the amplitude response that is caused by multipath components. Figure 2.13 shows the comparison of the simulated and measured reflection coefficient of the MEMS-based HIS. The reflection amplitude shows a good agreement between measured and simulated results which indicate that the resonance frequency shifts with the angle of incidence. The difference of the range of the reflection phase is caused most probably by two reasons: the inaccuracy of the needed calibration length that is used to retrieve true phase response and the non-ideality (non-planarity of the surface due to the mechanical processing) of the aluminum plate that is used to calibrate out the phase response of the HIS.

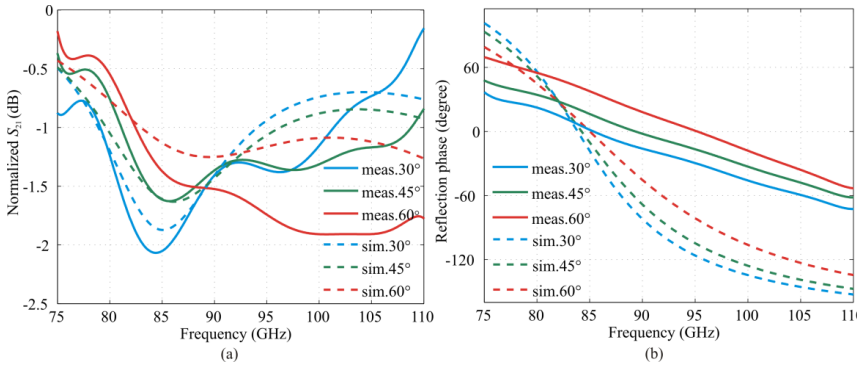

Figure 2.13 Measured reflection coefficient of the MEMS-based HIS: (a) amplitude; (b) phase [II].

3. Design and Optimization of Reconfigurable Reflectarray Element

3.1 Reconfigurable Reflectarray

The concept of a reflectarray was first described and experimentally verified in 1963 using square waveguide [40]. The reflectarray combines certain features and performance of the reflector and array antennas. In [40], the phase variation was achieved by introducing short-circuited termination into different depths of the waveguide sections to collimate waves from the feed antenna. The reflectarray has attracted more interest since the development of microstrip patch antennas in 1990's [41], [42] due to its light weight, flatness and conformity. When the elements of reflectarray are dynamically controlled (herein refer to the phase shift), the radiation characteristics could be manipulated accordingly. There are many techniques enabling active reconfiguration of the phase shift of the reflectarrays, which depends on the maturity, performance, and desired frequency range. For the phase tuning, various elements were used, e.g. varactor diodes at 5.8 GHz [43] and in *C*-band [44], MEMS switches at 12 GHz [45], p-i-n diodes at 60 GHz [46] and liquid crystal at 77 GHz [47].

A project focusing on silicon based MMID system for imaging, sensing and wireless communication applications was carried out between the Aalto University and VTT during 2010-2013 [4]-[6]. In this project, a system for MMID application was studied and especially 120 GHz reflectarrays and related methods for design, simulation, and measurement were studied. The research in this section provides an alternative solution to the design of reflectarray elements in which SU-8 is used as the dielectric substrate material.

3.2 Reflectarray Geometry Design

3.2.1 Element Design

The antenna element design of the reflectarray employs the principle of coplanar patch antenna (CPA) together with the conductor-backed coplanar waveguide (CB-CPW) technology [48], [49].

The proposed element has a 50 μm-thick layer of SU-8 photoresist as a substrate and two metallic layers on the opposite sides of the substrate. It is realized for a 2x2 mm² sized cell and targeting the 120 GHz frequency. The element spacing is 0.8λ at 120 GHz, and the first grating lobe appears when the theoretical steered angle is 14.5°. However, the element spacing is seen adequate for the anticipated application [6]. A patch antenna is etched on the upper ground layer and a 50-Ω coplanar waveguide (CPW) feed line having a signal strip of width W_f and a gap of width G_f. The resonant frequency of the CB-CPA element is preliminarily determined by the length of the patch L_p being the half the guided wavelength λ_g (see Figure 3.1). When the center frequency is determined, the impedance matching can be realized by adjusting the width of the patch W_p. Figure 3.1 shows the proposed geometry of the conductor-backed coplanar patch antenna (CB-CPA) element without the phase shifter.

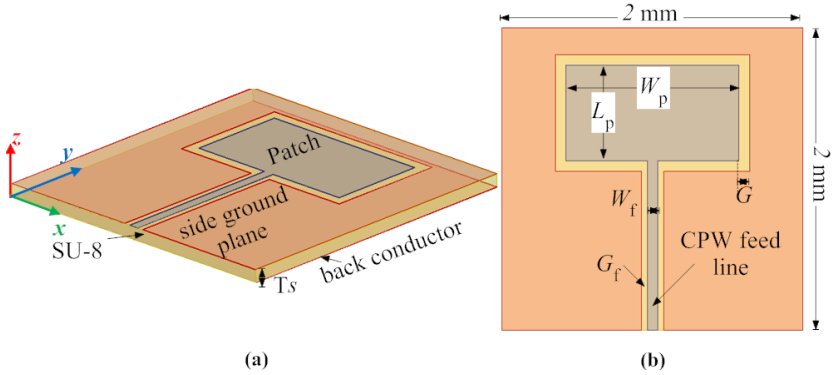

Figure 3.1 The geometry of the CB-CPA element (not to scale, the salmon pink color and gray color represent the metal portion, and the yellow color presents the etched slots): (a) 3D view; (b) front view [III].

3.2.2 SU-8 Photoresist Measurement

The dielectric properties of SU-8 at millimeter wavelengths are studied in few references, e.g., in [50]-[52]. There, the dielectric permittivity of SU-8 is reported to be 3.10-3.25 and its loss tangent 0.027-0.05. The substrate

material properties are sensitive to the particular lithographic fabrication process and may vary due to, e.g., the residual water absorbed in the material. The dielectric properties of the SU-8 substrate are characterized with on-wafer measurements and a test structure is fabricated on a silicon wafer with a 50-μm layer of SU-8 on it. The coplanar lines are 10-mm long and their characteristic impedance is from 34 Ω to 52 Ω. Figure 3.2 depicts the test structure. The measured permittivity is 3.0 and loss tangent is 0.03 at 120 GHz. For details of the SU-8 results see [III].

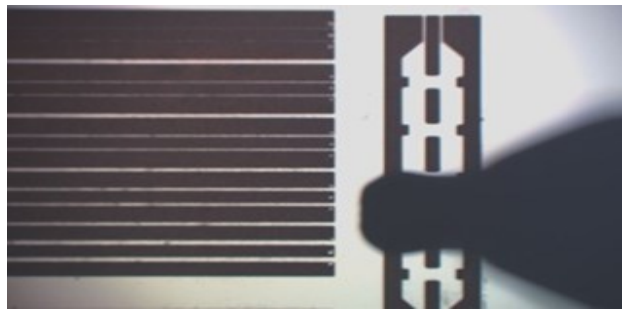

Figure 3.2 The ends of the fabricated CB-CPW lines. The gap of the lines increases from 5 μm to 40 μm from top down. The center conductor has width of 96 μm. Also the on-wafer probe is seen in lower right corner of the figure [III].

3.2.3 Active MEMS Phase Shifter

An electrostatically activated phase shifter with three capacitive shunt type MEMS switches on a CB-CPW line will be integrated into the antenna element (see Figure 3.3(a)). The phase shifter is a one-port reflection type device wherein the phase delay is doubled per unit length depending on the location of the switches. Switching is achieved by applying a DC voltage of ca. 30 V between the membrane and CPW line. The MEMS phase shifter provides four discrete phase states by activating only one of three switches at a time. Practically, the phase shifter is coupled to the free space only through the antenna. See [III] for detail descriptions of the phase shifter.

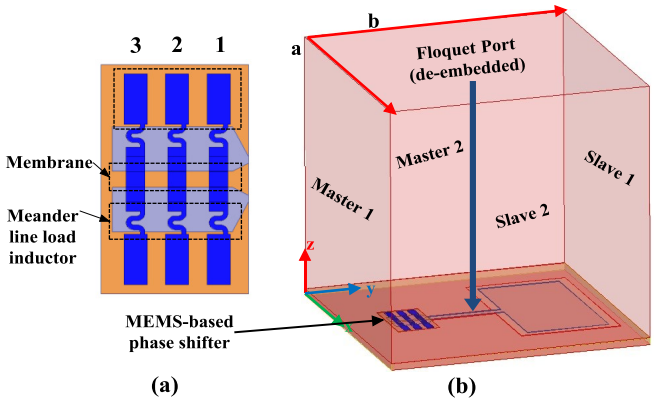

Figure 3.3 The HFSS model for a reflectarray element: (a) MEMS-based phase shifter; (b) The geometry and Floquet-port excitation, *E*-direction is along *y*-axis [III].

3.3 Reflectarray Performance Evaluation

The performance of the element is numerically analyzed in an array environment at the frequency of interest. In the simulation environment, the unit cell structure integrated with MEMS-based phase shifter is placed into the computational domain and periodic boundary conditions are used to simulate the infinite array of similar elements in two directions (*x*- and *y*-directions). A Floquet port is excited at 1.25 mm above the antenna element and de-embedded on the element surface (see Figure 3.3(b)). A parametric function consisting four discrete states is added to the simulation. Only one polarization is considered and *E*-direction is along *y*-axis.

The modulation efficiency of the reflectarray element is defined as:

$$\eta_m = \frac{|E_m|^2}{|E_m|^2 + |E_0|^2} \tag{3.1}$$

where $|E_m|^2$ is the power density of the field reflected from the phase shifter and $|E_m|^2 + |E_0|^2$ is the total reflected power density [4]. The modulation efficiency is calculated from the full-wave simulation result of reflectarray element and this could be affected by several design parameters, i.e.:

A. Effect of the patch width W_p (impedance matching),

B. Effect of the length of CPW feed line L_f between antenna patch and MEMS phase shifter,

C. Effect of the element spacing *W*.

The efficiency studies are carried out using the three above-mentioned design parameters shown in Table 3.1. When one design parameter is studied, other parameters are kept unchanged as nominal, unless mentioned otherwise.

Table 3.1 Nominal design parameters and geometric dimensions of the array element [III].

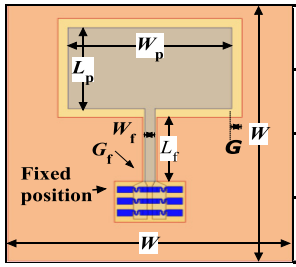

W	L_f	W_p	L_p
2000 μm	500 μm	1150 μm	630 μm
W_f	G	G_f	
70 μm	70 μm	15 μm	

Figure 3.4 illustrates the constellation diagram produced by the antenna element in the bore-sight direction with four different W_p lengths for four discrete phase shifts. The markers which evenly distribute on the fitted circle represent four discrete phase states. The origin of the fitted circle represents the specular reflection of the electric field E_o and the radius of the fitted circle represents the absolute value of the modulated field E_m. The array modulation efficiency is also presented in Figure 3.4 according to the calculation using Eq. (3.1). More results and discussion regarding the performance affected by other parameters can be seen in [III].

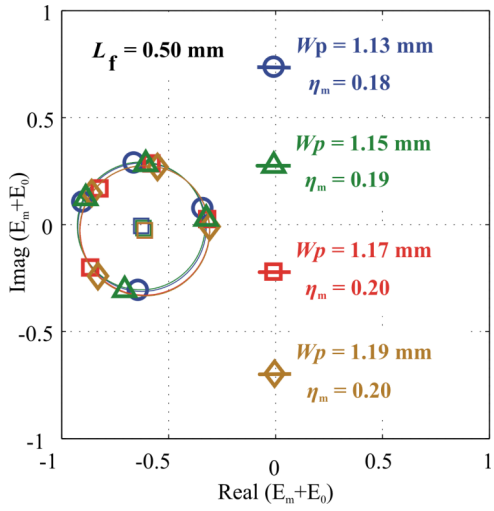

Figure 3.4 Simulated S_{11}-parameter with four discrete switching states with four different patch widths W_p at 120 GHz [III].

4. Development of Methods for Antenna Measurement

Antenna measurement refers to the experimental verification of the AUT specifications and parameters. Typical parameters of antennas include radiation pattern, directivity, polarization, gain, phase, etc. Research in antenna measurement field include a wide range topics which comprises of antenna measurement in non-anechoic environments, frequency versus time-domain analysis, near-field to far-field transformation, compact antenna test range, etc.

The most common and conventional method is the far-field antenna measurement where the AUT is placed in the far-field range of the reference antenna. The transmission between the AUT and the reference antenna is then recorded at different rotations of the AUT. Due to the requirement for testing a large antenna in a relatively small space, the near-field method was developed. In the near-field measurement technique, the near-field of the AUT is sampled spatially with a suitable probe antenna moving over the measurement surface. The measured near-field distribution is then used to calculate the antenna far-field radiation properties [53]. Another common method is the compact antenna test range (CATR) for accurate measurements of electrically large antennas at millimeter and submillimeter wavelengths. The CATR uses a collimating element to transform a spherical wavefront into a plane wave. In principle, any antenna could be successfully measured by the aforementioned method with proper implementation. However, the options of choosing one method over the other depend on the surrounding environment, facility cost, and the electrical dimensions of the AUT, etc. Furthermore, each measurement technique has certain advantages and limitations.

The research described in this section deals with certain limitations occurred during the antenna measurement processes (see Section 1.1). In Section 4.1, a new technique is proposed to process the antenna far-field measurements obtained in non-anechoic sites to obtain equivalent free space radiation

patterns. In Section 4.2, a new method is proposed to retrieve the antenna radiation pattern from reflection coefficient measurements avoiding AUT movement and connecting cables. In Section 4.3, a new technique is presented to realize a wideband hologram CATR.

4.1 Generation of Radiation Pattern from Non-Anechoic Measurements

Conventional antenna measurements are carried out in anechoic chambers. The purpose of employing an anechoic chamber is to eliminate the reflected field components emanating from the measurement enclosures so that the measured radiation pattern corresponds to that in free space conditions. Recently, signal-processing methods have been employed to further improve the quality of the data measured in moderately good anechoic conditions [15]-[17]. However due to practical and monetary constraints it is not always possible to emulate a perfect anechoic environment. The failure of the chamber to provide a purely free space environment affects the measurement accuracy. The objective then is to study methods that may eliminate the undesired reflections measured in non-anechoic conditions through further processing of the measured data. This is generally completed by time gating method, which transforms the frequency domain response into time domain data and filter out the delayed time pulses which are caused by multi-path interferences [54], [55]. A traditional FFT (Fast Fourier Transform)-based method has been investigated to be very efficient for removing undesired signals [56]. Some other techniques may also be applied [57]-[61], e.g. instead of the Fourier transform, matrix-pencil method is utilized for obtaining the time response of the measured frequency domain data [57], [58] and for radiation pattern error corrections [59]. An oversampled Gabor transform is utilized to identify and remove the reflected signals on the ground from the measured frequency response [17]. Such aforementioned procedures would make antenna measurements much easier and more cost-effective.

This section is organized as follows. The measurement scheme and procedure are presented in Section 4.1.1. In Section 4.1.2 the traditional FFT-based method to eliminate the unwanted reflection is introduced. Section 4.1.3 presents the proposed method using Chebyshev polynomial.

4.1.1 Description of the Measurement Scheme

All the measurements presented in this research have been obtained using a far-field measurement system housed in an anechoic chamber of dimensions 10×7.5×8.5 m^3. A simplified scheme of the whole measurement system is shown in Figure 4.1. The probe and the AUT are separated by a distance d_p, and a metal plate is placed in a parallel separation d_m from the AUT/probe to model a non-anechoic reverberant chamber. Here, we use a single antenna for both transmitter and receiver but instead of carrying out measurements at a single frequency, we use a band of frequencies to carry out the measurements. This band of frequencies at which the characteristics are to be measured, should be quite narrow and one should ensure that the antenna characteristics do not change over this band. The objective for performing measurements in a finite frequency band is to transform this finite bandwidth frequency domain data to the time domain where the various undesired reflections can be eliminated through time gating.

The measurement campaign was carried out in the frequency domain, measuring the $S_{21}(f)$ *H*-plane parameter of the two horn transmit-receive system in the band of interest for each azimuth angle ϕ from −90° to 90° at step of 1°. The FFT-based method relates the time domain and frequency domain. The time delay (*TD*) is defined as the time between the arrivals of the direct and reflected signals. Therefore, to better distinguish the main contribution from the AUT and the diffraction from the reflector, the minimum bandwidth (*BW*) should be determined as $BW=1/TD$. In this research, the bandwidth of 0.6 GHz, ranging from 3.05 GHz to 3.65 GHz was used in the measurement. The center frequency is 3.35 GHz.

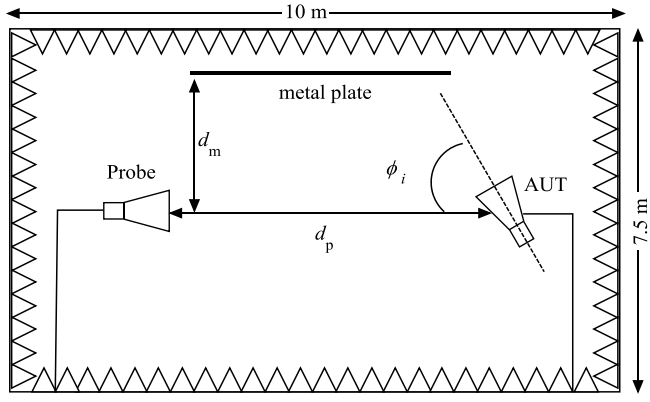

Figure 4.1 A top view of the antenna measurement system.

4.1.2 FFT-Based Method

The traditional methods achieve the reduction of the reflected and diffracted fields using the FFT-based method, which describes the impulse response of the reverberant chamber from its frequency response by using the inverse Fourier transform [56]. In the time domain, the direct contribution from the transmitter to the receiver is detected and gated, eliminating the undesired echoes through the use of low-pass filters. Applying the Fourier transform to this new gated time domain response provides only the direct contribution and thus the radiation pattern can be retrieved at the frequency of interest. Here, the various steps of the FFT-based method are summarized as follows and the result reconstruction is shown in Figure 4.2 (detailed procedure and results can be seen in [IV]):

1) Measure the coherent (amplitude/phase) frequency response covering the bandwidth from 3.05 GHz to 3.65 GHz.

2) Apply the inverse FFT to $S_{21}(f,\phi)$ to obtain the temporal response $S_{21}(t,\phi)$.

3) Once in the time domain, the direct contribution between the transmitting and the receiving antenna is approximately retained and the unwanted signals can be gated by truncating the waveform beyond a time based on the shortest path from the AUT to the probe in the presence of the reflector:

$$t = 2\sqrt{\left(d_{\mathrm{p}}/2\right)^2 + d_{\mathrm{m}}^2}\Big/c \tag{4.1}$$

for the current measurement setup, the parameters are $d_{\mathrm{p}} = 7.7$ m, $d_{\mathrm{m}} = 2$ m, and c is the velocity of light (3×10^8). Therefore, $t = 28.92$ ns.

4) Transforming the truncated data to the frequency domain by applying the FFT one obtains the processed frequency domain $S_{21}'(f,\phi)$ response.

One can observe that most of the reflection and diffracted fields in the azimuth angle range of −20°...−60° are reduced. However, one of the problems is that the quality of the results depends on the available bandwidth of the measurement. For this reason, we introduce a new method in the next section.

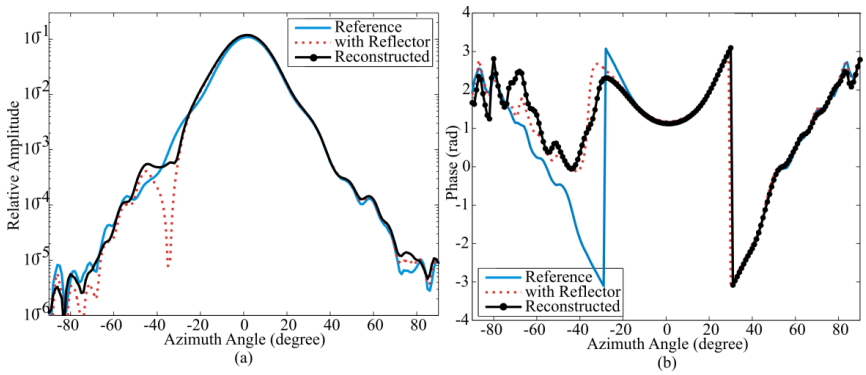

Figure 4.2 Result of the reconstruction using the FFT-based method: (a) pattern; (b) phase [IV].

4.1.3 Chebyshev Polynomial Method

It has been observed in earlier studies [62]-[64] that when scaled versions of the Bessel functions are used to approximate any causal time domain data, the frequency domain response can be fitted by the analytical transforms of the scaled Bessel functions (Chebyshev polynomials of the first and second kinds [65], [66]). The numerical value of the coefficients obtained by fitting the frequency domain data by the various orders of Chebyshev polynomials of the first and second kinds follow the trend of the time domain waveforms, even though the time domain waveforms are being approximated by scaled Bessel functions [62]-[64]. Therefore, the plot of the coefficients multiplying the scaled Bessel functions of the first kind will be able to distinguish between the various reflections and will help one to accomplish the separation between the direct wave and the various reflections present in a non-anechoic measurement.

In this new procedure, one starts with the measured data $S_{21}(f,\phi)$ as described in Section 4.1.1. The measurements are performed for different azimuth angles ϕ_i. For each azimuth angle, a set of data for different frequencies from f_1 to f_{M2} are measured simultaneously (marked as $X(f_1)...X(f_{M2})$). Correspondingly, a set of different coefficients a_n for different angles can be obtained by solving the matrix of Eq. (4.2) through the application of the conjugate gradient method (CGM) [67], where M_2 the number of frequency domain data, N-1 is is the number of the maximum degree in the polynomials. $\varphi_n(f, l_2)$ in Eq. (4.2) is represented in Eq. (4.3), l_2 is the frequency scaling factor and is chosen to be slightly larger than the maximum bandwidth of the available measurement data. T_n and U_{n-1} are

Chebyshev polynomials of the first and second kind. See [IV], [66] for detailed interpretation of Eqs. (4.2) and (4.3).

$$\begin{bmatrix} \mathrm{Re}\begin{pmatrix} \varphi_0(f_1,l_2) & \varphi_1(f_1,l_2) & \cdots & \varphi_{N-1}(f_1,l_2) \\ \varphi_0(f_2,l_2) & \varphi_1(f_2,l_2) & \cdots & \varphi_{N-1}(f_2,l_2) \\ \vdots & \vdots & \vdots & \vdots \\ \varphi_0(f_{M_2},l_2) & \varphi_1(f_{M_2},l_2) & \cdots & \varphi_{N-1}(f_{M_2},l_2) \end{pmatrix} \\ \mathrm{Im}\begin{pmatrix} \varphi_0(f_1,l_2) & \varphi_1(f_1,l_2) & \cdots & \varphi_{N-1}(f_1,l_2) \\ \varphi_0(f_2,l_2) & \varphi_1(f_2,l_2) & \cdots & \varphi_{N-1}(f_2,l_2) \\ \vdots & \vdots & \vdots & \vdots \\ \varphi_0(f_{M_2},l_2) & \varphi_1(f_{M_2},l_2) & \cdots & \varphi_{N-1}(f_{M_2},l_2) \end{pmatrix} \end{bmatrix}_{2M_2\times N} \begin{bmatrix} a_0 \\ a_1 \\ \vdots \\ a_{N-1} \end{bmatrix}_{N\times 1} = \begin{bmatrix} \mathrm{Re}\begin{pmatrix} X(f_1) \\ X(f_2) \\ \vdots \\ X(f_{M_2}) \end{pmatrix} \\ \mathrm{Im}\begin{pmatrix} X(f_1) \\ X(f_2) \\ \vdots \\ X(f_{M_2}) \end{pmatrix} \end{bmatrix}_{2M_2\times 1} \tag{4.2}$$

$$\varphi_n(f,l_2)=\frac{2i(-i)^n}{n}\left[\left(i\sqrt{1-\left(\frac{2\pi f}{l_2}\right)^2}\right)U_{n-1}\left(\frac{2\pi f}{l_2}\right)+T_n\left(\frac{2\pi f}{l_2}\right)\right]. \tag{4.3}$$
$$\text{for } |2\pi f| < l_2$$

For the FFT-based method, truncation is made in the time domain to eliminate the reflection and diffraction of the fields to be measured. In this new approach, the truncation is made to the Chebyshev series. We truncate the series when the scaled Bessel function of a certain order peaks at the time at which we would like to truncate the temporal function to prevent reflections or other secondary fields creeping in. For the detailed procedure, see [IV]. The result of the reconstruction is shown in Figure 4.3. When using the Chebyshev polynomial to fit the measured data and then truncating the series, the corresponding mean squared error between the reference antenna pattern and the reconstructed one is approximately 0.066 when the observation angle is limited from −90° to 0° and is 0.057 when the complete set of azimuth angle is considered from −90° to 90°. The mean squared error between the reference and the reconstructed results using different methods are summarized in Table 4.1. Hence, it appears that at least for this data set, the present method is more robust. By comparing Figure 4.2(b) to Figure 4.3(b), it is seen that the proposed method provides a more realistic phase response for the AUT.

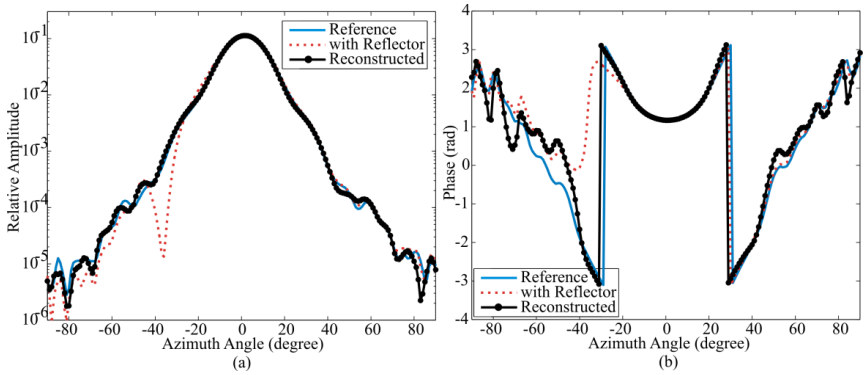

Figure 4.3 Result of the reconstruction using Chebyshev Polynomials: (a) pattern; (b) phase [IV].

Table 4.1 The norm of the mean squared error between the free space results and the data processed using different methods [IV].

Azimuthal Angular Range	Bandwidth: 0.6 GHz	
	FFT	Chebyshev
−90°... 0°	0.186	0.066
−90°... 90°	0.148	0.057

4.2 Antenna Pattern Retrieval from Reflection Coefficients

The antenna pattern is measured in the far-field or near-field, or in a compact antenna test range (as described in the background of Section 1.1). There are certain limitations to the aforementioned methods. In any method, the antennas are connected to the measurement equipment with cables that, when moved or rotated, easily change their properties. Several techniques for measuring the phase errors caused by flexing cables are discussed in [68]. At high frequencies, even a small relative change in the geometry of dimensions of the cable may cause a huge phase change to the transmitted signal, because the cable can be electrically very long. Although the error compensation techniques have been introduced [69], the measurement errors due to bending cables may be significant especially in the planar near-field scanning at high frequencies.

Some antennas, such as RFID (radio-frequency identification) antennas, are typically attached directly to an RFID chip and there is no possibility for a cable connection. Then, the antenna radar cross section (RCS) measurement technique can be used to characterize the antenna [70]-[73]. This method avoids the problems related to flexing cables, but it requires a potentially large far-field antenna range. Small millimeter wave antennas are often integrated on chip and traditional antenna measurement techniques have limitations in measurements on a probe station. The conventional methods are based on spherical measurement requiring complex mechanical arms for the probe antenna movements around the AUT [74]-[82]. The near-field wire-scattering method presented in [83] may not need the rotating cables but is capable to solve only one pattern cut.

In this section, a new antenna radiation pattern retrieval method using reflection coefficients results is proposed. It avoids flexing cables and AUT movements during the measurement procedure. Section 4.2.1 presents the equations relating the properties of the reflective load to the measured reflection coefficient. Section 4.2.2 presents the simulation and experimental setup for the verification. The 1D and 2D antenna patterns solved from reflection coefficients are presented in Section 4.2.3.

4.2.1 Reflection Coefficients and Antenna Aperture Field

In this method, the reflection coefficient of an antenna is measured when the antenna is placed close to a reflecting surface, whose reflection properties vary spatially in a known way. The measurement is repeated with different reflective surfaces, for example moving the reflective surface over the antenna

between each measurement. After an adequate amount of information is gathered, the near-field distribution of the antenna is solved from the measured reflection coefficients and the known reflector properties. Figure 4.4 shows the schematic layout of the pattern retrieval process.

The reflection coefficient is related to the properties of the reflective load by using the plane wave spectrum method and can be calculated as

$$S_{11,\text{aperture}} = \frac{\iint_S E_\Gamma(x,y,z=0)\,E_{\text{AUT}}(x,y,z=0)\,dxdy}{\iint_S E_{\text{AUT}}(x,y,z=0)\,E^*_{\text{AUT}}(x,y,z=0)\,dxdy} \tag{4.4}$$

$$S_{11} = S_{11,\text{static}} + e^{2\,(j\theta_d - \alpha)} S_{11,\text{aperture}} \tag{4.5}$$

where * denotes the complex conjugate. For convenience, the symbols used in the equations and figures are summarized with their descriptions in Table 4.2. Particularly, the reflection coefficient contains a constant term $S_{11,\text{ static}}$ due to the impedance mismatch between the antenna and the generator, and due to environmental reflections. This term is assumed independent of the varying reflective load. For a detailed explanation and derivation of the equations, see [V], [VI].

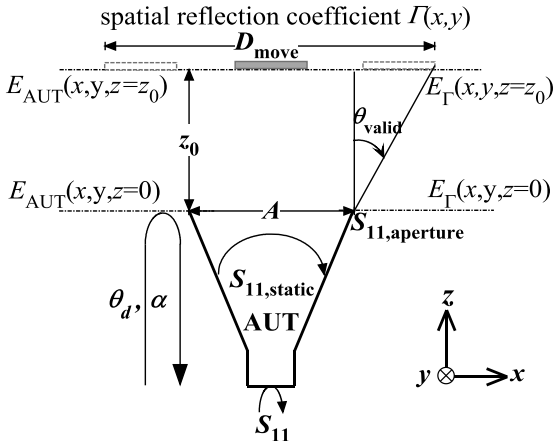

Figure 4.4 Layout of the proposed antenna pattern retrieval method [V], [VI].

Table 4.2 Symbols and descriptions [VI].

Symbol	Description
$E_{AUT}(x, y, z)$	electrical aperture field distribution at the plane z
$E_r(x, y, z)$	field reflected from the reflective surface at the plane z
z_0	offset distance
S	aperture surface
$S_{11,aperture}$	reflection coefficient referenced to the aperture plane of a lossless and perfectly matched antenna
S_{11}	reflection coefficient referenced to the antenna feed
θ_d, α	the phase delay and the attenuation constant between the antenna feed and aperture plane
$S_{11,n}$	the nth simulated reflection coefficient
$A_{initial}$, $\theta_{initial}$	initial guess of the amplitude and phase
A, B	aperture dimensions of the horn antenna

4.2.2 Simulations and Experiments

The proposed method is tested experimentally and by simulations using a Ka-band pyramidal horn antenna operating at 30 GHz as the AUT. The simulation setup is shown in Figure 4.5. The PEC strip is placed vertically in parallel to the antenna aperture, moved along x-direction, additionally, for 2D simulation, after the first movement, the strip is placed horizontally and moved along y-direction, see [V] for details. The reflection coefficients are recorded at each discrete position of the strip. It is important to select the distance z_0 and D_{move} such that the evanescent modes generated by the AUT are weak enough at the reflective plane and the reflection from the reflective plane is strong enough to be detected by the AUT.

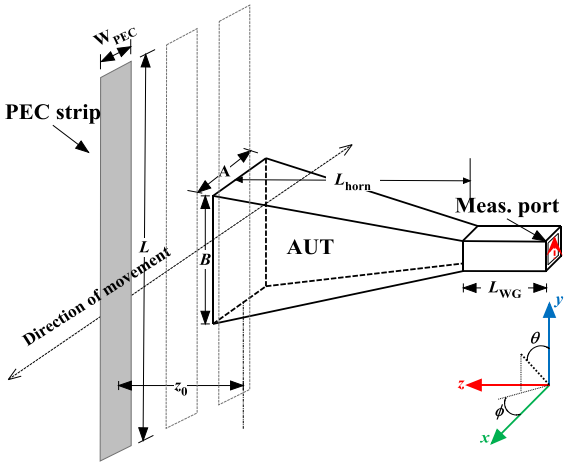

Figure 4.5 Simulation setup, see [V] for the details of the pyramidal horn dimensions and photograph of the corresponding experimental setup (not to scale).

4.2.3 Solving the Antenna Aperture Field

After the adequate number of reflection coefficients are gathered, the antenna aperture field E_{AUT} is determined by finding the minimum of the least-squares fitting in Eq. (4.6), which is solved iteratively using the quasi-Newton method starting from the initial guess for the aperture near-field given as Eq. (4.7). Figure 4.6 shows the comparison of the reconstructed, simulated and measured normalized radiation patterns at 30 GHz. Normally we choose values with uniform amplitude and phase and normalize this electric field distribution to unity, hence, $A_{\mathrm{initial}} = 1$, $\theta_{\mathrm{initial}} = 1$.

$$\Delta = \min_{E_{\mathrm{AUT}},\alpha} \sum_n \left| S_{11,\mathrm{aperture}}\left(E_{\mathrm{AUT}}, \Gamma_n(x,y)\right) e^{-2\alpha} + S_{11,\mathrm{static}} - S_{11,n} \right|^2 \quad (4.6)$$

$$E_{\mathrm{AUT}}(x,y,z=0) \begin{cases} A_{initial} e^{j\theta_{\mathrm{initial}}} & \text{when } |x| < \frac{A}{2} \text{ and } |y| < \frac{B}{2} \\ 0 & \text{elsewhere} \end{cases} \quad (4.7)$$

where θ_d is omitted because the phase delay term is embedded into the unknown complex aperture field. In addition, the field can be spatially limited according to the physical aperture of the antenna and full reflection is assumed from the reflective surface and zero reflection elsewhere.

For 2D determination, we assume that the near-field distribution is separable, i.e. the total field can be represented as a product of field distribution in two orthogonal directions. Two sets of measurement are performed in horizontal direction and vertical direction respectively. According to the method introduced in [V], the aperture field distributions of two orthogonal directions are solved separately. The 2D aperture field is then calculated accordingly [VI]. Figure 4.7 shows the comparison of the contour plot of the antenna far-field pattern at 30 GHz. The grey color and dashed-line rectangular in Figure 4.6 and 4.7 are the valid angular regions defined from the measurement setup [V], [VI].

These results show that the proposed method is suitable for characterizing certain types of antennas without a need for a traditional two-way measurement. The measurement accuracy provided already by these initial results seems adequate for certain purposes. There may be also a possibility to extend this method to characterize small antennas on a probe station.

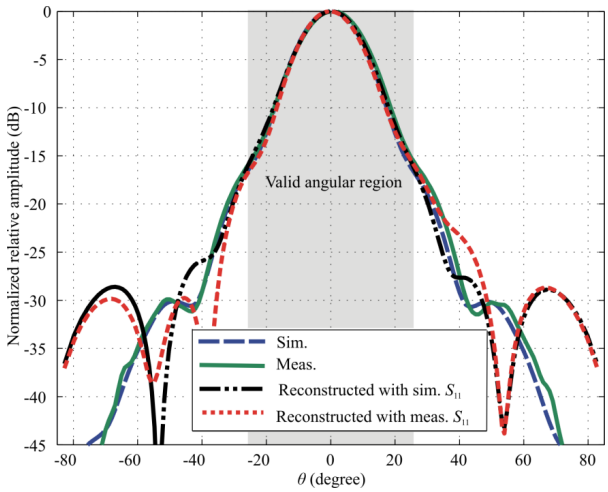

Figure 4.6 Normalized far-field pattern at 30 GHz [V].

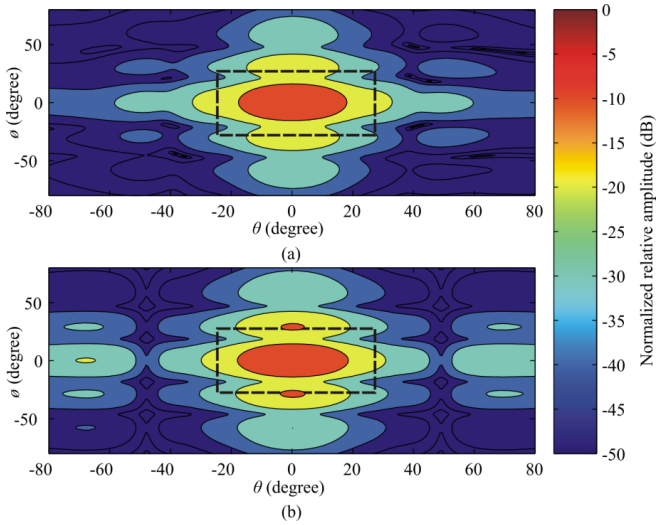

Figure 4.7 Normalized 2D far-field pattern at 30 GHz: (a) simulated; (b) reconstructed with simulated reflection coefficient [VI]. The dashed-line rectangular represents the valid angular region.

4.3 Realization of Wideband Hologram Compact Antenna Test Range

A CATR transforms a spherical wave into a plane wave in a very short distance (compared to the generally known far-field limit of $2D^2/\lambda$) using a collimating element, which can be a reflector [84], a lens [85], [86], or a hologram [90]. For a reflector, the surface accuracy is typically required to be better than 0.01 λ and even 0.007 λ for a large reflector [87], [88]. E.g., at 1 THz one hundredth of the wavelength is 3 μm, which may be too stringent to be manufactured in large scale. The hologram-based CATR (HCATR) was developed to produce a plane wave for antenna measurement at mm/submm-wave frequency [89], [90]. There are several types of hologram, e.g. a reflection-type amplitude hologram [91], a transmission-type phase hologram [92] and a reflection-type phase hologram [93]. As a transmission-type element, the accuracy becomes considerably less stringent than for a reflector [26]. Manufacturing of a hologram is easier than that of a reflector surface because of the two-dimensional planar structure. Consequently, the HCATR is very attractive for antenna measurement at mm/submm-wave bands. E.g., the antenna pattern measurement of Odin-telescope at 119 GHz was reported in [18]. A large HCATR was constructed and tested at 322 GHz [21], [22]. A 1.5-m reflector antenna (Admirals RTO) was tested in a HCATR at 650 GHz [23], [25]. However, as a frequency sensitive element, the operating bandwidth is usually limited to around ± 5%-10% [26].

In this section, we present a technique to overcome the limitation of the narrow bandwidth. The feed location needs to be adjusted on the axis for compensating the wavefront phase curve of the feed according to the Fresnel approximation. Particularly, Section 4.3.1 shows the derivation process of the wideband HCATR formulas. In Section 4.3.2 the experimental setup and performance are presented to verify the technique.

4.3.1 Derivation of Wideband Formulas

For a transmittance hologram, the interference pattern varies with the path difference between the feed and the plane wave field as:

$$c(x,y) = \sqrt{x^2 + y^2 + F^2} - x\sin\theta_c \tag{4.8}$$

where point (x, y) is located in the hologram, F denotes the focal length and θ_c indicates the direction of plane wave propagation. When $F >> |x|$ and $F >> |y|$, the square root can be approximated as the second order Taylor series:

$$c(x,y) \approx F + \frac{x^2+y^2}{2F} - \frac{(x^2+y^2)^2}{8F^3} - x\sin\theta_c . \tag{4.9}$$

For the given wavelength λ, if the focal ratio (F/D_H) is large enough [VII], the phase can be approximated as the first order Taylor series as:

$$\phi(x,y) = \frac{2\pi}{\lambda}c(x,y) \approx \frac{2\pi}{\lambda}(F + \frac{x^2+y^2}{2F} - x\sin\theta_c) \tag{4.10}$$

where D_H is the diameter of the hologram. When the wavelength is scaled down by M and the feed is moved further away to the distance MF, the equation would be:

$$\phi'(x,y) = \frac{2\pi}{\lambda}\left[M^2F + \frac{x^2+y^2}{2F} - xM\sin\theta_c'\right]. \tag{4.11}$$

The second term in both Eqs. (4.9) and (4.10) is the same for producing a plane wave. The first term is independent of (x, y) with respect to the hologram collimation. The last term implies the new direction of the plane wave propagation. Therefore, the feeding location and plane wave direction for a new frequency can be formulated as follows:

$$\begin{cases} F' = \dfrac{\lambda}{\lambda/M}F = MF \\ \theta' = \arcsin(\dfrac{\sin\theta_c}{M}) \end{cases}. \tag{4.12}$$

A wideband HCATR can be realized with the same aperture only by linearly adjusting the feeding location on the axis. Figure 4.8 illustrates the layout of the proposed adjusting procedure.

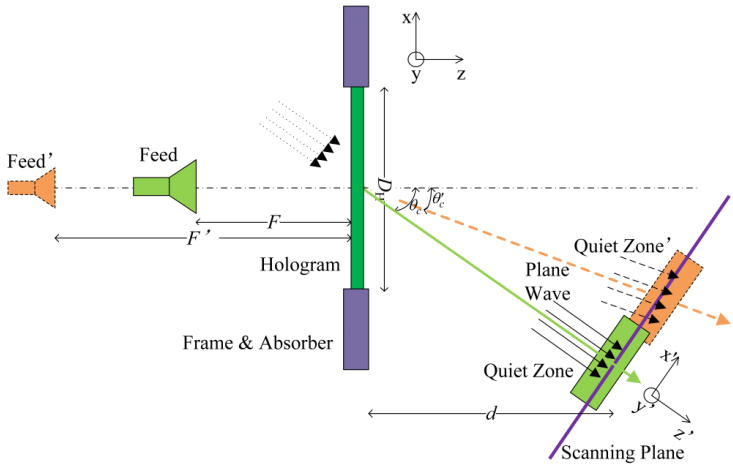

Figure 4.8 Layout of the proposed wideband HCATR [VII].

4.3.2 Experimental Verification and Performance

An experimental wideband HCATR has been designed and built for the verification of the proposed method. The hologram is quantized into the binary code for fabrication and the size is 350 mm × 350 mm (detailed description in [VII]). An optimized weighting is utilized to the hologram to achieve desired relative flat amplitude and phase distribution [VII], [90].

The experimental measurement setup for tests at 95 GHz and 170 GHz is shown in Figure 4.9. For 95 GHz, the off-axis angle is $\theta c = 39.5°$ and the distance between the hologram and the quiet-zone d = 1050 mm. The corrugated horn is placed at F = 1432 mm from the hologram along its normal direction. For 170 GHz, the parameters are $\theta'c = 39.5°$ and F' = 2562 mm. More details are presented in [VII].

The performance is evaluated by the peak-to-peak (PP) deviation from the flat amplitude and phase response in the quiet-zone. Figure 4.10 shows the measured co-polarized field for horizontal polarization in horizontal line at 95 GHz and 170 GHz respectively. The amplitude is normalized to the maximum. The measured result of the co-polarized quiet-zone fields are summarized in Table 4.3 (H denotes the horizontal polarization and V denotes the vertical polarization). For results and discussion of other polarization and cut, see [VII].

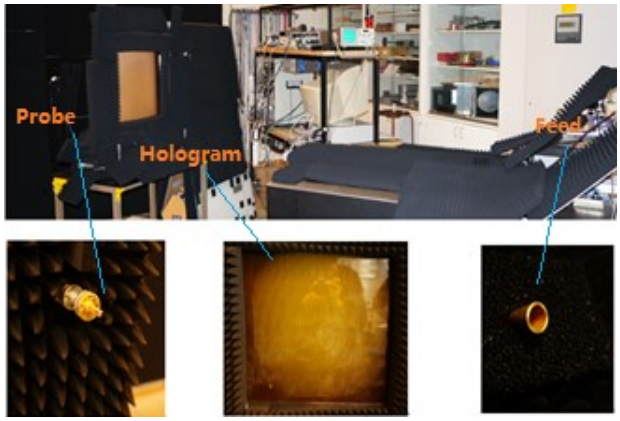

Figure 4.9 The setup of the HCATR for the measurements (top), open-ended waveguide probe (bottom left), the hologram (bottom middle), and the D-band corrugated horn as the CATR feed (bottom right) [VII].

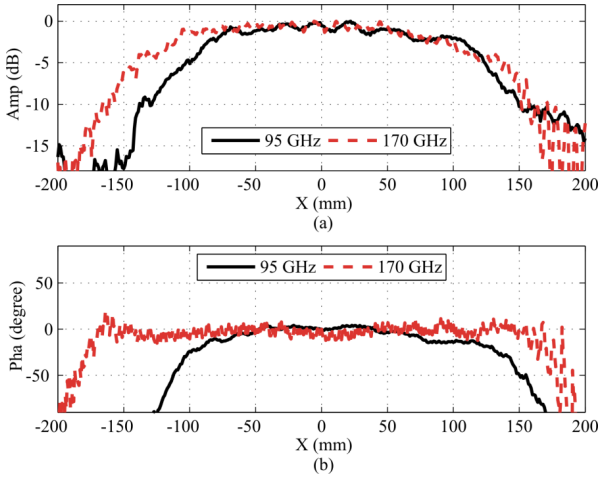

Figure 4.10 The measured quiet-zone field with horizontal polarization in the horizontal line (y = 0, step = 1.0 mm at 95 GHz, and 0.8 mm at 170 GHz in the scanning x-axis): (a) amplitude; (b) phase [VII].

Table 4.3 The measured quiet-zone quality of the wideband hologram CATR: PP deviations from the planar field (amplitude in dB, phase in degrees) [VII].

Frequency (GHz)	PP value in horizontal line				PP value in vertical line			
	H polarization		V polarization		H polarization		V polarization	
	Amp.	Pha.	Amp.	Pha.	Amp.	Pha.	Amp.	Pha.
85	1.6	18.2	2.4	22.8	1.4	13.2	1.1	11.6
95	1.7	10.8	1.9	16.4	1.7	12.8	1.5	8.8
170	1.9	20	2.1	22.6	2.1	11.4	1.5	9

5. Summary of the Publications

I. "Millimeter wave beam steering with a MEMS-based high impedance surface"

Beam steering with a MEMS-based high impedance surface has been studied in W band. The steering mechanism is based on the principle of a phase gradient array. Reflection phase properties of a single unit cell structure are analyzed. Radiation pattern of a strip consisting of elements with different impedance is analyzed numerically for two beams of normal and oblique incidence. The steering range is achieved from -45° to 45° with respect to the normal direction.

II. "Reflection phase characterization of the MEMS-based high impedance surface"

The reflection properties of the MEMS-based HIS illuminated from oblique angles of incidence have been characterized numerically, and a quasi-optical measurement setup has been built for experimental characterization. The resonance frequency and the relative bandwidth are slightly increasing with the increase of the angle of incidence. The comparison between the simulated and measured results is discussed.

III. "Design and optimization of reconfigurable reflectarray element with MEMS phase shifter"

The design and optimization process of reconfigurable reflectarray element with MEMS-based phase shifter at 120 GHz is presented. The dielectric properties of SU-8 substrate are characterized with on-wafer measurements. Several design parameters which affect the element efficiency are studied. Through proper design and optimization of the array element the reasonable

element efficiency can be achieved by utilizing SU-8 photoresist as its substrate.

IV. "Generation of free space radiation patterns from non-anechoic measurements using Chebyshev polynomials"

Generally, antenna radiation patterns are measured in an anechoic condition so that the presence of undesired reflections does not skew the final measurements. The objective of this paper is to search for methods which can extract meaningful approximate results from non-anechoic measurements. The Chebyshev polynomials are used to process the data collected under non-anechoic environment and to generate a radiation pattern equivalent to that in free space conditions. The problem with this method is that some *a priori* information is required about the environment. Measured data has been used to illustrate the applicability of this new method and its improved performance over the FFT-based methods.

V. "Antenna pattern retrieval from reflection coefficient measurements with reflective loads"

This paper presents a new method for antenna pattern retrieval from reflection coefficient measurements. A reflective load with known reflective properties is placed close to the aperture of the antenna under test. The reflection coefficient at the antenna feed is measured with multiple different reflective loads. The antenna pattern is then solved from the measurements with an inversion method. This paper derives and verifies the analytical foundations needed to implement the method, and demonstrates the method both by simulations and experiments for a pyramidal horn antenna at 30 GHz.

VI. "2D antenna radiation pattern retrieval using reflection coefficient measurement"

This paper reviews the antenna radiation pattern retrieval method using reflection coefficient measurement developed in [V], and extension for two-dimensional apertures is proposed. This is achieved sweeping a PEC strip in front of the antenna aperture in two orthogonal directions instead of previously used one direction. The method has been demonstrated by simulation for a pyramidal horn antenna at 30 GHz.

VII. "Realization of wideband hologram compact antenna test range by linearly adjusting the feed location"

This paper describes a wideband hologram-based CATR: which can be realized by linearly adjusting the feed location. The position needs to be adjusted for approximately compensating the wave front curve of the feed, which is proportional to the operating frequency. The theory can be conformed under the paraxial condition. For the acceptable quiet-zone field quality over a wide band, the large focal ratio is required. The idea is verified and the wideband performance of the quiet-zone is studied with the simulated and measured results at W band (95 GHz) and D band (170 GHz).

6. Conclusions and Future Work

This dissertation contributes to the development of methods for antenna measurement, and numerical and experimental characterization of quasi-optical components, i.e. MEMS-based HIS and reflectarray element.

The reflection properties of the single unit cell structure of MEMS-based HIS was studied, tunability of the MEMS varactors and beam steering of a large structure at 80 GHz has been demonstrated with a simplified model [I]. The reflection phase across the surface can be programmed to produce a phase gradient, which allows steering the reflected beam within the range from -45° to +45°. A quasi-optical measurement setup has been built for the experimental characterization [II]. Future work would be addressed to development of the fabrication process for a reliable actuation of the large array of the MEMS varactors.

The design and optimization process of the reconfigurable reflectarray element integrated with MEMS-based phase shifter at 120 GHz has been studied [III]. Also, the dielectric properties of SU-8 substrate have been characterized with on-wafer measurements. Several design parameters which could affect the modulation efficiency have been studied. The element spacing (size of the side ground plane) has very significant influence to the modulation efficiency. Through proper design and optimization of the array element, reasonable modulation efficiency could be achieved by utilizing SU-8 photoresist as its substrate.

Several new methods have been proposed to deal with certain limitations during antenna measurements. Particularly, a new technique using the Chebyshev polynomials has been proposed to process the antenna measurements obtained in non-anechoic sites to obtain equivalent free space radiation patterns in [IV]. This new technique combines the principle of a FFT-based method with the special relationship between coefficients of the Bessel-Chebyshev polynomials. The assumption of this technique is that the minimum distance from the transmitter to the receiver through the reflector is

known. If the antenna radiation pattern is complicated and has many large sidelobes, it would be very difficult to recover all the signals. Also the performance of the proposed method depends on how well the scaling factor is chosen. Sample experimental result is presented to demonstrate the potential of this approach over conventional time gating techniques for a certain class of problems. Future research interest would be how to find an automated way to truncate the series of the coefficients based on the measured data and not on the *a priori* knowledge of the environment.

In [V] and [VI], a new antenna pattern retrieval method is proposed. In this method, the antenna reflection coefficient is measured multiple times when a unique reflective load with known spatial reflection properties is placed near the antenna in each measurement. The antenna pattern is obtained from the measurements with an inversion algorithm. The analytical equations for equating the antenna reflection coefficient to the near-field load of the antenna have been presented. Simulations have been used to verify the theoretical basis and the method has been experimentally demonstrated at 30 GHz. The results show that the method could enable sufficient accuracy with low gain antennas or in the vicinity of main lobe with directive antennas. This method requires optimization, and the typical time to retrieve the field depends on the selected cost function and optimization algorithm. Therefore, future research interests include: improve the inversion method, optimize the reflective surface, study the influence of the initial guess to the retrieved field, and extend the current method to a probe station to measure an integrated antenna.

In [VII], a new method for a wideband operation of the hologram-based CATR has been presented. The wideband formulas for linearly adjusting the feed have been discussed and verified. The performance of the wideband operation has been demonstrated by measurements at W (95 GHz) and D (170 GHz) bands with the hologram aperture diameter of 350 mm. When the bandwidth is increased, the direction of the plane wave propagation is varied more. The direct beam starts to disturb the desired planar wavefront at the higher end of the frequency band, while at the lower end the quiet-zone size is getting smaller. Future research would be addressed to study the possible bandwidth limit and minimum of hologram configurations required for the proposed technique.

Reference

[1] C. A. Balanis, *Antenna Theory: Analysis and Design*, Third Edition, New York: Wiley, 2005.

[2] G. Rebeiz, *RF MEMS: Theory, Design, and Technology*, Hoboken, NJ: John Wiley & Sons, Inc., 2004.

[3] "ECC decision of 19 March 2004 on the frequency band 77-81 GHz to be designated for the use of automotive short range radars," *European Commission Decision* no. 2004/545/EC, Retrieved June 9, 2014.

[4] A. Tamminen, J. Ala-Laurinaho, D. Gomes-Martins, J. Häkli, P. Koivisto, M. Kärkkäinen, S. Mäkelä, P. Pursula, P. Rantakari, M. Sipilä, J. Säily, R. Tuovinen, M. Varonen, K. A. I. Halonen, A. Luukanen, and A. V. Räisänen, "Reflectarray for 120-GHz beam steering application: design, simulations, and measurements," in *Proc. SPIE Passive and Active Millimeter-Wave Imaging XV*, Baltimore, USA, Apr. 23, 2012, p. 836205.

[5] A. Tamminen, *Developments in imaging at millimeter and submillimeter wavelengths*, Doctoral dissertation, Dept. of Radio Science and Engineering, Aalto University, Espoo, Finland, 2013.

[6] A. Tamminen, S. Mäkelä, J. Ala-Laurinaho, J. Häkli, P. Koivisto, P. Rantakari, J. Säily, A. Luukanen, and A. V. Räisänen, "Reflectarray design for 120-GHz radar application: measurement results," *IEEE Trans. Antennas Propag.*, vol. 61, no.10, pp. 5036-5047, Oct. 2013.

[7] D. Chicherin, *Studies on microelectro-mechanically tuneable high-impedance surface for millimeter wave beam steering*, Doctoral dissertation, Dept. of Radio Science and Engineering, Aalto University, Espoo, Finland, 2011.

[8] J. Ala-Laurinaho, D. Chicherin, Z. Du, C. Simovski, T. Zvolensky, A. V. Räisänen, M. Sterner, Z. Baghchehsaraei, U. Shah, S. Dudorov, J. Oberhammer, A. V. Boriskin, L. Le Coq, E. Fourn, S. A. Muhammad, R. Sauleau, A. Vorobyov, F. Bodereau, G. El Haj Shhade, T. Labia, P. Mallejac, J. Åberg, M. Gustafsson, and T. Schier, "TUMESA-MEMS tuneable metamaterials for smart wireless applications," in *Proc. 7th European Microw. Integrat. Circ. Conf.,* Amsterdam, the Netherlands, Oct. 29-30, 2012, pp. 95-98.

[9] D. Chicherin, M. Sterner, Z. Baghchehsaraei, J. Oberhammer, S. Dudorov, Z. Du, T. Zvolensky, A. Vorobyov, M. de Miguel Gago, E. Fourn, R. Sauleau, T. Labia, G. El Haj Shhade, F. Bodereau, P. Mallejac, J. Åberg, C. Simovski, and A. V. Räisänen, "MEMS tunable metamaterials for beam steering millimeter wave applications," in *Proc. NATO Research Workshop on Advanced Materials Technologies for Micro/Nano-devices, Sensors, and Actuators: From*

Fundamentals to Applications, St. Petersburg, Russia, June 29 – July 2, 2009, p. 45.

[10] A. V. Räisänen, J. Ala-Laurinaho, D. Chicherin, Z. Du, A. Generalov, A. Karttunen, D. Lioubtchenko, J. Mallat, A. Tamminen, and T. Zvolensky, "Antennas for electronic beam steering and focusing at millimeter wave lengths," in *Proc. Int. Conf. Electromagnetics in Advanced Applications,* Cape Town, South Africa, Sep. 2-7, 2012, pp. 1235-1237.

[11] A. V. Räisänen, J. Ala-Laurinaho, D. Chicherin, Z. Du, A. Generalov, A. Karttunen, D. Lioubtchenko, J. Mallat, A. Tamminen, and T. Zvolensky, "Beam-steering antennas at millimeter wavelengths," in *Proc. 5th Global Symp. Millimeter Waves*, Harbin, China, May 27-30, 2012, pp. 170-173.

[12] Z. Du, D. Chicherin, and A. V. Räisänen, "Beam steering with MEMS-based HIS on a lossy sillicon substrate at 80 GHz," in *The Millimetre Wave Days: The 6th ESA Workshop on Millimetre-Wave Technology and Applications*, Espoo, Finland, May 23-25, 2011.

[13] J. Ala-Laurinaho, Z. Du, V. Viikari, and A. V. Räisänen, "Radiation pattern retrieval from impedance measurement with a reflective object in the antenna near field," in *Proc. IEEE Int. Conf. Antenna Meas. & Application* (*2014 IEEE CAMA*), Antibes Juan-les-Pins, France, Nov. 16-19, 2014.

[14] V. Viikari, Z. Du, V. Semkin, J. Ala-Laurinaho, and A. V. Räisänen "Reflection coefficient method for characterizing antennas on probe stations," in *Proc. 9th European Conf. Antennas Propag.,* Lisbon, Portugal, Apr. 12-17, 2015.

[15] B. Fourestie, Z. Altman, and M. Kanda, "Anechoic chamber evaluation using the matrix pencil method," *IEEE Trans. Electromagn. Compat.*, vol. 41, no. 3, pp. 169-174, Aug. 1999.

[16] B. Fourestie, Z. Altman, and M. Kanda, "Efficient detection of resonances in anechoic chambers using the matrix pencil method," *IEEE Trans. Electromagn. Compat.,* vol. 42, no. 1, pp. 1-5, Feb. 2000.

[17] B. Fourestie and Z. Altman, "Gabor schemes for analyzing antenna measurements," *IEEE Trans. Antennas Propag.*, vol. 49, no. 9, pp. 1245-1253, Sep. 2001.

[18] T. Sehm, J. Ala-Laurinaho, T. Hirvonen, and A. V. Räisänen, "Antenna measurements using a hologram CATR," *Electron. Lett.*, vol. 35, no. 10, pp. 757-758, May 1999.

[19] J. Ala-Laurinaho, *Numerical studies on a radio frequency hologram and its use in antenna measurements*, Doctoral dissertation, Dept. of Electrical and Communications Engineering, Helsinki University of Technology, Espoo, Finland, 2001.

[20] J. Ala-Laurinaho, T. Hirvonen, P. Piironen, A. Lehto, J. Tuovinen, A. V. Räisänen, and U. Frisk, "Measurement of the Odin telescope at 119 GHz with a hologram-type CATR," *IEEE Trans. Antennas Propag.,* vol. 49, no. 9, pp. 1264-1270, Sep. 2001.

[21] J. Häkli, T. Koskinen, A. Lönnqvist, J. Säily, J. Mallat, J. Ala-Laurinaho, V. Viikari, J. Tuovinen, and A. V. Räisänen, "Testing of a 1.5 m reflector antenna at 322 GHz in a CATR based on a hologram," *IEEE Trans. Antennas Propag.*, vol. 53, no. 10, pp. 3142-3150, Oct. 2005.

[22] A. Lönnqvist, T. Koskinen, J. Häkli, J. Säily, J. Ala-Laurinaho, J. Mallat, V. Viikari, J. Tuovinen, and A. V. Räisänen, "Hologram-based compact range for submillimeter-wave antenna testing," *IEEE Trans. Antennas Propag*., vol. 53, no. 10, pp. 3151-3159, Oct. 2005.

[23] T. Koskinen, J. Ala-Laurinaho, J. Säily, A. Lönnqvist, J. Häkli, J. Mallat, J. Tuovinen, and A. V. Räisänen, "Experimental study on a hologram-based compact antenna test range at 650 GHz," *IEEE Microw. Theory Techn.* vol. 53, no. 9, pp. 2999–3006, Sep. 2005.

[24] J. Ala-Laurinaho, J. Häkli, A. Karttunen, T. Koskinen, A. Lönnqvist, J. Mallat, E. Noponen, A. Tamminen, M. Vaaja, V. Viikari, A. V. Räisänen, and J. Lemanczyk, "Tests of a 1.5-m reflector antenna in a 650 GHz hologram CATR," in *Proc. 2nd European Conf. Antennas Propag.,* Edinburgh, UK, Nov. 11-16, 2007, pp. 1-6.

[25] A. Karttunen, J. Ala-Laurinaho, M. Vaaja, T. Koskinen, J. Häkli, A. Lönnqvist, J. Mallat, A. Tamminen, V. Viikari, and A. V. Räisänen, "Antenna tests with a hologram-based CATR at 650 GHz," *IEEE Trans. Antennas Propag*., vol. 57, no.3, pp. 711-720, Mar. 2009.

[26] T. Hirvonen, J. Ala-Laurinaho, and A. V. Räisänen, "Performance analysis of a submillimeter wave hologram CATR," in *Proc. 27th European Microw. Conf.*, Jerusalem, Israel, Sep. 8-12, 1997, pp. 681-686.

[27] D. Sievenpiper, *High-impedance electromagnetic surfaces*, Ph.D. dissertation, Dept. of Electrical Engineering, University of California, Los Angeles, USA, 1999.

[28] D. Sievenpiper, L. Zhang , R. F. J. Broas, N. G. Alexopolous, and E. Yablonovitch, "High-impedance electromagnetic surfaces with a forbidden frequency band," *IEEE Trans. Microw. Theory Techn.,* vol. 47, no. 11, pp. 2059-2074, Nov. 1999.

[29] R. F. J. Broas, D. F. Sievenpiper, and E. Yablonovitch, "A high-impedance ground plane applied to a cellphone handset geometry," *IEEE Trans. Microw. Theory Techn., vol.* 49, no. 7, pp. 1262-1265, July 2001.

[30] D. Sievenpiper, J. Schaffner, R. Loo, G. Tangonan, S. Ontiveros, and R. Harold, "A tunable impedance surface performing as a reconfigurable beam steering reflector," *IEEE Trans. Antennas Propag.,* vol. 50, no. 3, pp. 384-390, Mar. 2002.

[31] D. Sievenpiper, J. Schaffner, B. Loo, G. Tangonan, R. Harold, J. Pikulski, and R. Garcia, "Electronic beam steering using a varactor-tuned impedance surface," in *Proc. IEEE AP-S Int. Symp. Antennas Propag.,* Boston, USA, July 8-13, 2001, vol. 1, pp. 174-177.

[32] D. Sievenpiper and J. Schaffner, "Beam steering microwave reflector based on electrically tunable impedance surface," *Electron. Lett.,* vol. 38, no. 21, pp. 1237-1238, Oct. 2002.

[33] D. F. Sievenpiper, J. H. Schaffner, H. J. Song, R. Y. Loo, and G. Tangonan, "Two-dimensional beam steering using an electrically tunable impedance surface," *IEEE Trans. Antennas Propag.,* vol. 51, no. 10, pp. 2713-2722, Oct. 2003.

[34] S. Tretyakov, *Analytical Modeling in Applied Electromagnetics*, Boston: Artech House, 2003.

[35] D. Chicherin, S. Dudorov, D. Lioubtchenko, V. Ovchinnikov, S. Tretyakov, and A. V. Räisänen, "MEMS-based high-impedance surfaces for millimeter and

submillimeter wave applications," *Microw. Opt. Technol. Lett.,* vol. 48, no. 12, pp. 2570-2573, Dec. 2006.

[36] D. Chicherin, M. Sterner, J. Oberhammer, S. Dudorov, J. Åberg, and A. V. Räisänen, "Analog type millimeter wave phase shifters based on MEMS tunable high-impedance surface in rectangular metal waveguide," in *Proc. IEEE MTT-S Int. Microw. Symp.,* Anaheim, USA, May 23-28, 2010, pp. 61-64.

[37] M. Sterner, D. Chicherin, J. Åberg, R. Sauleau, A. Räisänen, G. Stemme, and J. Oberhammer, "Integration of microwave MEMS reconfigurable reflective surfaces in rectangular waveguide stubs," in *Proc. Asia-Pacific Microw. Conf.*, Yokohama, Japan, Dec. 7-10, 2010, pp. 1825-1828.

[38] D. Chicherin, M. Sterner, D. Lioubtchenko, J. Oberhammer, and A. V. Räisänen, "Analog-type millimeter-wave phase shifters based on MEMS tunable high-impedance surface and dielectric rod waveguide," *Int. J. Microw. Wireless Techn.,* vol. 3, no. 5, pp. 533-538, Oct. 2011.

[39] D. Chicherin, S. Dudorov, D. Lioubtchenko, V. Ovchinnikov, and A. V. Räisänen, "Characterisation and measurements of a multilayer high-impedance surface at W-band", *Proc. 1st Int. Congr. on Advanced Electromagnetic Materials in Microwave and Optics*, Oct. 22-26, 2007, Rome, Italy, pp. 891-894.

[40] D. Berry, R. Malech, and W. Kennedy, "The reflectarray antenna," *IEEE Trans. Antennas Propag*., vol. 11, no. 6, pp. 645-651, Nov. 1963.

[41] R. D. Javor, X. D. Wu, and K. Chang, "Design and performance of a microstrip reflectarray antenna," *IEEE Trans. Antennas Propag*., vol. 43, no. 9, pp. 932-939, Sep. 1995.

[42] J. Huang and J. A. Encinar, *Reflectarray Antennas*, New Jersey, USA: Wiley, 2007.

[43] S. V. Hum, M. Okoniewski, and R. J. Davies, "Realizing an electronically tunable reflectarray using varactor diode-tuned elements," *IEEE Microw. Compon. Lett.,* vol. 15, no. 6, pp. 422-424, June 2005.

[44] M. Riel and J. Laurin, "Design of an electronically beam scanning reflectarray using aperture-coupled elements," *IEEE Trans. Antennas Propag*., vol. 55, no. 6, pp. 1260-1266, May 2007.

[45] J. Perruisseau-Carrier and A. K. Skrivervik, "Monolithic MEMS-based reflectarray cell digitally reconfigurable over a 360 degree phase range," *IEEE Antennas Wireless Propg. Lett.,* vol. 7, pp. 138-141, Feb. 2008.

[46] H. Kamoda, T. Iwasaki, J. Tsumochi, and T. Kuki, "60-GHz electrically reconfigurable reflectarray using p-i-n diode," in *Proc. IEEE MTT-S Int. Microw. Symp*., Boston, USA, June 7-12, 2009, pp. 1177-1180.

[47] S. Bildik, S. Dieter, C. Fritzsch, M. Frei, C. Fischer, W. Menzel, and R. Jakoby, "Reconfigurable liquid crystal reflectarray with extended tunable phase range," in *Proc. 41st European Microw. Conf.,* Manchester, UK, Oct. 10-13, 2011, pp. 404-407.

[48] K. Li, C. H. Cheng, T. Matsui, and M. Izutsu, "Coplanar patch antennas: principle, simulation and experiment," in *Proc. IEEE AP-S Int. Symp. Antennas Propag.,* Boston, USA, July 8-13, 2001, vol.3, pp. 402-405.

[49] R. Simons, *Coplanar Waveguide Circuits, Components, and Systems*, New York: John Wiley, 2001.

[50] F. D. Mbairi and H. Hesselbom, "High frequency design and characterization of SU-8 based conductor backed coplanar waveguide transmission lines," in *Proc. Int. Symp. Adv. Packaging Materials: Process, Properties & Interfaces*, Mar. 16-18, 2005, pp. 243-248.

[51] S. N. Dudorov, D. V. Lioubtchenko, and A. V. Räisänen, "Open resonator technique for measuring dielectric properties of thin films on a substrate," in *Proc. XXVIII URSI General Assembly*, 2005, paper no. A03.6.

[52] S. Arscott, F. Garet, P. Mounaix, L. Duvillaret, J. L. Coutaz, and D. Lippens, "Terahertz time-domain spectroscopy of films fabricated from SU-8," *Electron. Lett.*, vol. 35, no. 3, pp. 243-244, Feb. 1999.

[53] A. D. Yaghjian, "An overview of near-field antenna measurements," *IEEE Trans. Antennas Propag.,* vol. 34, no. 1, pp. 30-45, Jan. 1986.

[54] A. M. Predoehl and W. L. Stutzman, "Implementation and results of a time-domain gating system for a far-field range," in *Proc. 19th Annual Meeting Symp. AMTA,* Boston, USA, Nov. 1997, pp. 8-12.

[55] Y. T. Hsiao, L. Y. Y. Lin. Y. C. Lu, and H. T. Chou, "Applications of time-gating method to improve the measurement accuracy of antenna radiation inside an anechoic chamber," in *Proc. IEEE AP-S Int. Symp. Antennas Propag.*, Columbus, USA, June 22-27, 2003, vol. 3, pp. 794-797.

[56] S. Loredo, M. R. Pino, F. Las-Heras, and T. K. Sarkar, "Echo identification and cancellation techniques for antenna measurement in non-anechoic test sites," *IEEE Antennas Propag. Mag.,* vol. 46, no. 1, pp. 100-107, Feb. 2004.

[57] B. Fourestie, Z. Altman, J. Wiart, and A. Azoulay, "On the use of matrix-pencil method to correlate measurements at different test sites," *IEEE Trans. Antennas Propag.,* vol. 47, no. 10, pp. 1569-1573, Oct. 1999.

[58] T. K. Sarkar and O. Pereira, "Using the matrix pencil method to estimate the parameters of a sum of complex exponentials," *IEEE Antennas Propag. Mag.,* vol. 37, no. 1, pp. 48-55, Feb. 1995.

[59] G. Leon, S. Loredo, S. Zapatero, and F. Las Heras, "Radiation pattern error corrections based on matrix pencil method," in *Proc. IEEE AP-S Int. Symp. Antennas Propag.*, San Diego, USA, July 5-11, 2008.

[60] S. Loredo, G. Leon, R. G. Ayestaran, and F. Las-Heras, "Reconstruction of antenna radiation patterns from phaseless measurements in nonanechoic chambers," *IEEE Antennas Wireless Propag. Lett.*, vol. 10, pp. 1282-1285, Nov. 2011.

[61] R. G. Ayestarán, G. León, S. Loredo, J. López-Fernández, and F. Las-Heras, "Sparse deconvolution based on regularisation for echo correction in antenna measurement," *IET Microwaves Antennas Propag.,* vol. 6, no. 12, pp. 1299-1305, Sep. 2012.

[62] J. Koh, T. Kim, W. Lee, and T. K. Sarkar, "Extraction of wideband response using Bessel-Chebyshev functions," *IEICE Trans. Commun.*, vol. E85-B, no. 10, pp. 2263-2272, Oct. 2002.

[63] M. Yuan, J. Koh, T. K. Sarkar, W. Lee, and M. Salazar-Palma, "A comparison of performance of three orthogonal polynomials in extraction of wide-band response using early time and low frequency data," *IEEE Trans. Antennas Propag.*, vol. 53, no. 2, pp. 785-792, Feb. 2005.

[64] M. Yuan, A. De, T. K. Sarkar, J. Koh, and B. Jung, "Conditions for generation of stable and accurate hybrid TD-FD MoM solutions," *IEEE Trans. Microw. Theory Techn.,* vol. 54, no. 6, pp. 2552-2563, June 2006.

[65] M. Abramowitz and I. A. Stegun, *Handbook of Mathematical Functions*, New York: Dover, 1970.

[66] J. C. Mason and D. C. Handscomb, *Chebyshev Polynomials*, New York: Chapman & Hall/CRC, 2003.

[67] T. K. Sarkar, *Application of the Conjugate Gradient Method in Electromagnetics and Signal Processing*, New York: Elsevier Science Publications, 1991.

[68] D. Slater*, Near-field Antenna Measurements*, Norwood, MA: Artech House, 1991.

[69] J. Säily, P. Eskelinen and A. V. Räisänen, "Pilot signal-based real-time measurement and correction of phase errors caused by microwave cable flexing in planar near-field tests," *IEEE Trans. Antennas Propag.*, vol. 51, no. 2, pp. 195–200, Feb. 2003.

[70] D. D. King, "The measurement and interpretation of antenna scattering," *Proc. of the IRE*, vol. 37, no. 7, pp. 770-777, July 1949.

[71] W. Wiesbeck and E. Heidrich, "Wide-band multiport antenna characterization by polarimetric RCS measurements," *IEEE Trans. Antennas Propag.*, vol. 46, no. 3, pp. 341–350, Mar. 1998.

[72] J. Appel-Hansen, "Accurate determination of gain and radiation patterns by radar cross-section measurements," *IEEE Trans. Antennas Propag.*, vol. 27, no. 5, pp. 640-646, Sep. 1979.

[73] P. Pursula, M. Hirvonen, K. Jaakkola, and T. Varpula, "Antenna effective aperture measurement with backscattering modulation," *IEEE Trans. Antennas Propag.*, vol. 55, no. 10, pp. 2836–2843, Oct. 2007.

[74] T. Zwick, C. Baks, U. R. Pfeiffer, D. Liu, and B. P. Gaucher, "Probe based MMW antenna measurement setup," in *IEEE AP-S Int. Symp. Antennas Propag.,* June 20-25, 2004, vol. 1, pp. 747-750.

[75] J. A. G. Akkermans, R. Van Dijk, and M. H. A. J. Herben, "Millimeter-wave antenna measurement," in *Proc. of 37th European Microw. Conf.*, Munich, Germany, Oct. 9-12, 2007, pp. 83-86.

[76] K. V. Caekenberghe, K. M. Brakora, W. Hong, K. Jumani, D. Liao, M. Rangwala, Y. Z. Wee, X. Zhu, and K. Sarabandi, "A 2-40 GHz probe station based setup for on-wafer antenna measurements," *IEEE Trans. Antennas Propag.,* vol. 56, no. 10, pp. 3241-3247, Oct. 2008.

[77] S. Ranvier, M. Kyrö, C. Icheln, C. Luxey, R. Staraj, and P. Vainikainen, "Compact 3-D on-wafer radiation pattern measurement system for 60 GHz antennas," *Microw. Opt. Technol. Lett.,* vol. 51, no. 2, pp. 319-324, Feb. 2009.

[78] T. Ito, Y. Tsutsumi, S. Obayashi, H. Shoki, and T. Morooka, “Radiation pattern measurement system for millimeter-wave antenna fed by contact probe,” in *Proc. 39th European Microw. Conf.,* Rome, Italy, Sep. 29 - Oct. 1, 2009, pp. 1543-1546.

[79] S. Beer and T. Zwick, “Probe based radiation pattern measurements for highly integrated millimeter-wave antennas,” in *Proc. 4th European Conf. Antennas Propag*., Barcelona, Spain, Apr. 12-16, 2010.

[80] Y. Fu, T. P. Vuong, L. Dussopt, and F. Ndagijimana, “Characterization of integrated antennas at millimeter-wave frequencies,” in *Proc. 5th European Conf. Antennas Propag*., Rome, Italy, Apr. 11-15, 2011, pp. 160-163.

[81] K. Mohammadpour-Aghdam, S. Brebel, A. Enayati, R. Faraji-Dana, G. A. E. Vandenbosch, and W. Deraedt, “RF probe influence study in millimeter-wave antenna pattern measurements,” *Int. Journal of RF Microwave Computer-Aided Engineering*, vol. 21, no. 4, pp. 413-420, July 2011.

[82] D. Titz, F. Ferrero, G. Jacquemod, P. Brachat, and C. Luxey, “Measurement system for mm-wave integrated and probe-fed antennas,” in *Loughborough Antennas Propag. Conf.*, Loughborough, UK, Nov. 12-13, 2012.

[83] T. Calazans, H. D. Griffiths, A. L. Cullen, D. E. N. Davies, and R. Benjamin, “Antenna radiation pattern measurement using a near-field wire scattering technique,” *IEE Proc. Microwave Antennas Propag*., vol. 145, no. 3, pp. 263-267, June 1998.

[84] R. C. Johnson, H. A. Ecker, and R. A. Moore, “Compact range techniques and measurements,” *IEEE Trans. Antennas Propag.,* vol. 17, no. 5, pp. 568-576, Sep. 1969.

[85] A. D. Olver and A. A. Saleeb, “Lens-type compact antenna range,” *Electron. Lett.,* vol. 15, no. 14, pp. 409-410, July 1979.

[86] W. Menzel and B. Hunder, “Compact range for millimetre-wave frequencies using a dielectric lens,” *Electron. Lett.,* vol. 20, no. 19, pp. 768-769, Sep. 1984.

[87] “IEEE Standard Test Procedures for Antennas,” *ANSI/IEEE STD 149,* 1979.

[88] J. D. Huff, J. H. Cook, Jr., and B. W. Smith, “Recent developments in large compact range design,” in *Proc. AMTA,* Columbus, USA, Oct. 1992, pp. 5-39-5-44.

[89] J. Tuovinen, A. Vasara, and A. V. Räisänen, “A new type of compact antenna test range,” in *Proc. 22nd European Microw. Conf.* Espoo, Finland, Sep. 5-9, 1992, pp. 503-508.

[90] T. Hirvonen, J. Ala-Laurinaho, J. Tuovinen, and A. V. Räisänen, “A compact antenna test range based on a hologram,” *IEEE Trans. Antennas Propag*., vol. 45, no. 8, pp. 1270-1276, Aug. 1997.

[91] T. Koskinen, V. Viikari, J. Häkli, A. Lönnqvist, J. Ala-Laurinaho, J. Mallat, and A. V. Räisänen, “A reflection-type amplitude hologram as a collimating element in compact antenna test range,” in *Proc. 27th Annual AMTA Meeting Symp*., Newport, USA, Nov. 2005, pp. 417-421.

[92] J. Meltaus, J. Salo, E. Noponen, M. M. Salomaa, V. Viikari, A. Lönnqvist, T. Koskinen, J. Säily, J. Häkli, J. Ala-Laurinaho, J. Mallat, and A. V. Räisänen,

"Millimeter-wave beam shaping using holograms," *IEEE Trans. Microw. Theory Techn.,* vol. 51, no. 4, pp. 1274-1280, Apr. 2003.

[93] E. Noponen, J. Häkli, T. Koskinen, A. Lönnqvist, V. Viikari, J. Ala-Laurinaho, J. Mallat, and A. V. Räisänen, "Synthesis of reflection-type phase hologram for compact antenna test range at 310 GHz," in *Proc. 4th ESA Workshop on Millimetre-Wave Technology and Applications*, Espoo, Finland, Feb. 15-17, 2006, pp. 391-396.

Errata

Publication III

In the second paragraph of sub-section III. A, p. 2425, it should read "...calculated from equation (5)"

Publication IV

The unit of the colorbar in Fig. 4(a) and Fig. 6 should be "dB/10"

Eq. (5) should be

$$\phi_n(f,l_2)=\frac{2i(-i)^n}{n}\left[\left(i\sqrt{1-\left(\frac{2\pi f}{l_2}\right)^2}\right)U_{n-1}\left(\frac{2\pi f}{l_2}\right)+T_n\left(\frac{2\pi f}{l_2}\right)\right] \qquad \text{for } |2\pi f|<l_2$$

Eq. (6) should be

$$X\left(\frac{f}{l_2}\right)=\sum_{n=0}^{N}a_n\frac{2i(-i)^n}{n}\left[\left(i\sqrt{1-\left(\frac{2\pi f}{l_2}\right)^2}\right)U_{n-1}\left(\frac{2\pi f}{l_2}\right)+T_n\left(\frac{2\pi f}{l_2}\right)\right]$$

The dissertation presents three new methods to deal with certain limitations occurred during the antenna measurement processes. First, a new technique using the Chebyshev polynomials has been proposed to process the antenna measurements obtained in non-anechoic sites to obtain equivalent free space radiation patterns. Second, a new antenna pattern retrieval method from reflection coefficient measurements is proposed. Third, a new technique is presented to realize a wideband hologram compact antenna test range by linearly adjusting the feed location.
The dissertation also discusses characterization of quasi-optics, i.e. MEMS-based high-impedance surface (HIS) and reflectarray elements. First, the reflection properties of the unit cell structure of MEMS-based HIS is studied, and beam steering of a large structure at 80 GHz has been demonstrated with a simplified model. Second, the design and optimization process of reconfigurable reflectarray element integrated with MEMS-based phase shifter at 120 GHz is studied.

Aalto-DD 8/2015

ISBN 978-952-60-6049-1 (printed)
ISBN 978-952-60-6050-7 (pdf)
ISSN-L 1799-4934
ISSN 1799-4934 (printed)
ISSN 1799-4942 (pdf)

Aalto University
School of Electrical Engineering
Department of Radio Science and Engineering
www.aalto.fi

BUSINESS + ECONOMY

ART + DESIGN + ARCHITECTURE

SCIENCE + TECHNOLOGY

CROSSOVER

DOCTORAL DISSERTATIONS